

# AN APPROACH TO MODELLING FLASH-BOILING FUEL SPRAYS FOR DIRECT-INJECTION SPARK-IGNITION ENGINES

Christopher Price, Arash Hamzehloo and Pavlos Aleiferis\*

Department of Mechanical Engineering, Imperial College London, UK

David Richardson

Jaguar Land Rover, UK

\*Author for correspondence: Prof. Pavlos Aleiferis, Imperial College London, Department of Mechanical Engineering, Exhibition Road, London SW7 2AZ, UK, [p.aleiferis@imperial.ac.uk](mailto:p.aleiferis@imperial.ac.uk)

## ABSTRACT

*Flash-boiling is a phenomenon which occurs when a liquid is discharged into an environment with an ambient pressure below the saturation pressure of the liquid. The present computational work provides an approach to modelling flash-boiling fuel sprays using the Lagrangian particle tracking technique. An atomization model based on nucleation inside the nozzle is implemented as a boundary condition at the nozzle exit and alongside a superheat evaporation model for the emerging spray droplets. The near-nozzle dense spray region of flash-boiling sprays is also investigated by consideration to the initial spray plume cone angle. The model was able to predict important flash-boiling phenomenon such as spray collapse and droplet recirculation automatically, validated against experimental data.*

**KEYWORDS:** *Flash-boiling, spray droplet evaporation, direct-injection, spark-ignition engines.*

## NOMENCLATURE

### Latin Symbols

$A_d$	Droplet surface area [m <sup>2</sup> ]
$A_{eff}$	Effective nozzle orifice area due to cavitation [m]
$A_n$	Inner surface area of nozzle hole [m <sup>2</sup> ]
$C_p$	Specific heat coefficient [J/kgK]
$C_c$	Contraction coefficient
$C_d$	Discharge coefficient
$D$	Nozzle diameter [m]
$D_b$	Bubble departure diameter [m]
$D_d$	Droplet diameter [m]
$D_{eff}$	Effective nozzle diameter due to cavitation [m]
$D_i$	Binary Diffusivity Coefficient [m <sup>2</sup> /s <sup>2</sup> ]
$D_{ref}$	Reference bubble diameter [m]

$f$	Frequency of bubble departure [s <sup>-1</sup> ]
$F( *)$	Property function
$g$	Acceleration due to gravity [m/s <sup>2</sup> ]
$H_L$	Latent heat of vaporisation [J/Kg]
$L$	Nozzle length [m]
$m$	Mass of droplet [kg]
$\dot{m}$	Mass flow rate [kg/s]
$M_{sc}$	Subcooled evaporation rate [kg/s]
$M_{sh}$	Superheated evaporation rate [kg/s]
$M_t$	Total evaporation rate [kg/s]
$N_{ref}$	Reference nucleation site density [m <sup>-2</sup> ]
$N_{nuc}$	Nucleation site density [m <sup>-2</sup> ]
$N_{nuc}^*$	Dimensionless nucleation site density
$r$	Injector inlet corner radius [m]
$R$	Specific gas constant [J/kgK]

## Atomization and Sprays

$R_f$	Specific gas constant of droplet film [J/kgK]	$U$	Injection Velocity [m/s]
$R_{dia,cav}$	Initial droplet diameter reduction factor caused by cavitation	$U_{eff}$	Effective velocity at nozzle exit [m/s]
$R_{dia,flash}$	Initial droplet diameter reduction factor caused by flash-boiling	$U_{mean}$	In-nozzle mean velocity [m/s]
$T$	Ambient temperature [K]	$U_{vena}$	Velocity at vena contracta [m/s]
$T_d$	Droplet temperature [K]	$V_b$	Bubble volume [m <sup>3</sup> ]
$T_f$	Droplet film temperature [K]	$\dot{V}_t$	Total volumetric flow rate [m <sup>3</sup> /s]
$T_l$	Injection Temperature [K]	$\dot{V}_v$	Volumetric flow rate of vapour [m <sup>3</sup> /s]
$T_{ref}$	Reference Superheat Degree [K]	<b>Greek Symbols</b>	
$T_{sat}$	Saturation Temperature [K]		Heat transfer coefficient [W/mK]
$P$	Ambient pressure [Pa]	$\epsilon$	Void fraction
$P_i$	Upstream injection pressure [Pa]	"	Contact angle
$P_s$	Saturation pressure [Pa]	*	Dimensionless density function
$P_v$	Partial vapour pressure in computational cell [Pa]	$\rho_g$	Density of gas [kg/m <sup>3</sup> ]
$P_{vena}$	Pressure at vena contracta [Pa]	$\rho_l$	Density of liquid [kg/m <sup>3</sup> ]
$S_{nozzle}$	Internal surface area of nozzle [m <sup>2</sup> ]		Surface tension [N/m]
$Sh$	Sherwood number	$\Delta T$	Superheat degree [K]
			Dimensionless surface tension

# 1. INTRODUCTION

## 1.1 BACKGROUND

Flash boiling is a phenomenon which occurs when a liquid is discharged into an ambient environment with a pressure lower than its saturation pressure. This process is typically associated with very fast timescales due to the sudden pressure drop. The rapid reduction in pressure, and simultaneous increase in superheat cause the fuel to enter a metastable state with significant superheat thermal energy, which is consumed via the rapid flash-boiling process. Flash-boiling of fuel sprays can have a significant effect on spray formation and its characteristics, due to bubble nucleation, growth and phase change, producing explosive like atomization and complex collapsing spray structures (van Romunde and Aleiferis 2009; van Romunde *et al.*, 2007; Serras-Pereira *et al.*, 2010). Heterogeneous nucleation typically occurs at cavities such as dust particles, dissolved gas or wall boundaries and can occur inside, at and outside of the discharge orifice (Sher *et al.*, 2008). The effect of flash-boiling on the spray structure is difficult to predict, due to the rapid nature of flash-boiling. Zhang *et al.* (2011 and 2013) studied the liquid and vapour distribution in flash-boiling fuel sprays using planar laser induced exciplex fluorescence (PLIEF) and particle image velocimetry (PIV) techniques and found that increasing the superheat degree typically caused plumes from multi-hole injectors to merge into a single plume with highly concentrated fuel vapour and axial

momentum. The vortex ring which is found to develop at the spray tip region was shown to increase in strength pushing the plumes into the central axis, increasing axial velocity and penetration.

Flash-boiling of fuel sprays can occur under typical low-load spark-ignition engine operating conditions with fuel injection strategies in the intake stroke to promote 'homogeneous' mixture formation. Certain extreme engine design strategies such as heavy down-sizing and fully variable valve profiles are being investigated to increase thermal efficiency and meet the ever tightening carbon dioxide and toxic emission regulations. Some strategies involve early and rapid intake-valve closure, which can cause a sudden partial vacuum close to bottom dead centre intake that can lead to flash-boiling of the directly injected fuel spray. Highly volatile components of gasoline blends such as *n*-pentane can flash at even relatively high in-cylinder pressures (0.8–1.0 bar) especially if operating hot. It is the flashing of these high volatility components that drives the whole mechanism of gasoline spray collapse (van Romunde *et al.* 2007). Furthermore, the ever growing initiative to reduce the use of fossil fuels and the uncertainty associated with fuel supply, is causing a movement towards alternative fuel blends. Some of those contain bio-derived additives such as ethanol. Ethanol addition, even if in small percentages (10–20% per volume), leads to a highly increased vapour pressure of the blend that promotes flashing (Aleiferis *et al.*, 2010, 2015; Serras-Pereira *et al.*, 2012, 2013, 2015).

Flash boiling of gasoline fuel sprays in direct-injection engine applications can have a positive effect on air-fuel mixing, due to the increased evaporation rate and smaller droplet sizes (van Romunde and Aleiferis, 2013; Behringer *et al.*, 2014). However, depending on exact plume orientation and injector nozzle type, flashing and spray collapse may lead to decreased liner wall wetting but increased piston wall wetting due to increased axial momentum of the spray (Butcher *et al.*, 2015).

There has been a range of experimental research carried out on flash-boiling sprays in general over the last half century, whereby attempts have been made to characterise the phenomena of flashing both internally and externally, through many combinations of nozzle geometry, liquid type and ambient conditions. Early works by Sher and Elata (1977) and Kitamura *et al.* (1986) were carried out whereby empirical relationships for flashing sprays were developed, describing bubble growth rates, downstream droplet sizes and critical superheat degrees. The superheat degree ( $\Delta T$ ) refers to the difference between the droplet temperature and the fuels boiling temperature at a specific ambient pressure, and the critical superheat denotes the temperature difference that triggers the flashing mechanism. Sher *et al.* (2008) devised a review of the current understanding of flashing mechanisms, including bubble growth, intense nucleation and atomization. Although significant work has been undertaken on studying the concept of flash-boiling, experimental limitations have hindered a complete understanding of the complex physics involved. Due to typical nozzle diameters being in the range of 100–300  $\mu\text{m}$  and injection velocities ranging from 80–140  $\text{ms}^{-1}$  it is difficult to conduct experimental observations on in-nozzle flow and near nozzle regions. Some work has been completed on this aspect, whereby optical nozzles are developed to allow high speed imaging of in-nozzle flow. Several studies (Butcher *et al.*, 2013; Serras-Pereira *et al.*, 2010) have been carried out where optical nozzles have been developed and used to study fuel sprays experiencing both cavitation and flash-boiling. Cavitation and in-nozzle phase change via flash-boiling were visualised, however the difficulty of quantifying this was highlighted.

A subsequent effect of the experimental limitations is the difficulty in numerically modelling the phenomena, and hence the full potential of flash-boiling atomization is still being explored to this day. An interesting approach to numerically describe the in-nozzle flash-boiling phenomena is heterogeneous nucleation theory. This method is based on classical nucleation theory, where the

rate of metastable phase change is predicted. Homogeneous nucleation in the context of engine applications is often disregarded (Witlox and Bowen, 2002) due to the energy barrier for nucleation and bubble growth being sufficiently high. Whereas the energy barrier for heterogeneous nucleation is significantly lower due to the reduction of free energy needed for the onset of nucleation caused by surface features. A significant amount of work has been carried out on the topic of nucleation and bubble growth since the substantial work of Plesset and Zwick (1954) on the growth of vapour bubbles in a superheated liquid. Blander and Katz (1979) were among the first to investigate experimentally the onset of nucleation in pure liquids, finding that a large degree of superheat is needed (up to 90% of the critical temperature, *e.g.* 469.6 K for *n*-pentane) for homogeneous nucleation which was in agreement with classical nucleation theory. Nucleation in fuel injectors has been quantified by Li *et al.* (2015) and Zhang *et al.* (2015), where a 2-dimensional optical slit nozzle was manufactured to allow for a single layer of bubbles produced through nucleation to be photographed. This study documented nucleation via bubble number density and area void fraction at varying operating conditions.

In the context of in-nozzle bubble nucleation a developed model for predicting void development in flashing nozzle flows was proposed by Riznic and Ishii (1989) using a heterogeneous wall nucleation approach. This method was found to be able to predict the flashing phenomena relatively well, and matches experimental data sufficiently. One advancement away from previous attempts is the calculation of varying bubble number density, as opposed to the generally accepted constant evenly distributed assumption.

A second modelling approach proposed for nucleation in flashing flows was a two-paper sequence presented by Shin and Jones (1993) and Blinkov *et al.* (1993). In the former, a semi-empirical 1-dimensional model was developed to predict the onset of bubble nucleation in flashing nozzle flows. This included calculations for the number and size of bubbles per unit area from heterogeneous nucleation at varying superheats, allowing the downstream void to be calculated. The main source of energy was assumed to be transient conduction between the uniformly superheated liquid and vapor bubbles. The latter paper went on to investigate the accuracy of the developed model by comparison with experiment in a converging-diverging nozzle set-up. It was found that the model accurately predicted the void development, and thermal non-equilibrium was the dominating factor as opposed to mechanical non-equilibrium.

A third model proposed to predict in-nozzle properties is documented by Janet *et al.* (2015), whereby several analytical models were implemented into a Computational Fluid Dynamics (CFD) framework to produce a model with the capability of predicting downstream void fractions. Specifically, the nucleation site density was taken from Lemmert and Chawla (1977), the departure diameter from Kurul and Podowski (1991) and the departure frequency from Cole (1967). Janet *et al.* (2015) provide a detailed comparison between the three models described in a converging-diverging nozzle application where good agreement with experimental data was reported.

In-nozzle phase change and the resultant two-phase flow at the nozzle exit can hugely influence downstream spray characteristics such as penetration, liquid and vapour distribution and droplet properties. One parameter significantly influenced by flashing is the plume cone angle, specifically at close proximity to the nozzle orifice ( $0 < x/D < 20$ ). Due to vapour being present in the nozzle, a sudden expansion typically occurs upon being discharged into ambient, specifically at high injection pressures where an under-expanded jet can occur (Oza and Sinnamon, 1983). This rapid expansion of the vapour phase entrains liquid droplets (Kamoun *et al.* 2010) into the outer regions of the spray plume, evidently widening the cone angle. A number of other mechanisms can produce a radial widening of the plume, namely bubble bursting and inertial shattering (Oza and Sinnamon, 1983) as well as shock waves produced at choked conditions (Vieira and Simões-Moreira, 2007).

Another important phase-change phenomenon in high-pressure direct-injection nozzles is cavitation; this can occur due to pressure drop from geometrically-related effects or vortical structures in the bulk of the flow. Cavitation and flash-boiling are both phase-change phenomena, however the initiation mechanism is different. Cavitation is mechanically induced (through hydrodynamic forces), whereas flash-boiling is thermally induced (Brennen, 1995). Many experimental and modelling studies have been completed over the years and documented in the review of Schmidt and Corradini (2001). However, most of the previous work relates to diesel engine nozzles. Payri *et al.* (2004) studied the relationship between internal nozzle geometry, internal flow properties and spray characteristics for diesel injectors. A critical cavitation number was determined, allowing the relationship between injection parameters and injected mass to be modelled more accurately. Then Payri *et al.* (2005) documented a cavitation theory based on the contraction ratio and the resultant effective area of the nozzle exit, which in-turn affects the velocity and size of the injected spray droplets. Sarre *et al.* (1999) also developed a 1-dimensional cavitation model which predicts effective nozzle geometry and resultant droplet properties as a boundary condition at the nozzle exit. The model was validated against experimental data and showed a good prediction of discharge coefficient, as well as downstream spray characteristics. Delale *et al.* (2001) developed a quasi-1-dimensional model for the prediction of cavitating nozzle flows. Here a homogeneous bubbly mixture approach was applied, allowing for bubble-bubble interactions to be modelled as well as damping effects from liquid viscosity, thermal conduction and acoustic radiation. The developed model was able to predict nozzle flow characteristics accurately, even with a number of simplifying assumptions.

Currently there are limitations when it comes to modelling flash-boiling by CFD codes, as key flash-boiling mechanisms such as rapid evaporation and atomization cannot be easily captured. One of the latest attempts to model flash-boiling fuel sprays by CFD was conducted by Neroorkar and co-authors (Neroorkar *et al.* 2011; Neroorkar and Schmidt, 2011) in which an Eulerian approach was adopted to model a flashing spray emerging from a single-hole pressure-swirl injector. The results predicted contain features of spray collapse and provided useful insights, however, Eulerian simulations of sprays starting from inside the nozzle can be computationally very demanding if the modelling methodology needs to be applied in-cylinder for full-cycle engine simulations.

## **1.2 PRESENT CONTRIBUTION**

This paper makes an attempt to document the initial development of an Eulerian/Lagrangian methodology which is the ‘industry-standard’ approach to modelling liquid fuel sprays. The main aim was to improve the prediction of spray characteristics of flash-boiling fuel sprays for spark-ignition engines using multi-hole injectors. This work follows on from a recent publication by the current authors (Price *et al.*, 2015), whereby a superheated evaporation model was implemented by user coding in a commercial code (STAR-CD) and a parametric study was carried out to investigate the sensitivity of various sub-models and injection conditions to the behaviour of a typical multi-hole injector spray with and without flashing phenomena. The current work aims to contribute to the field of modelling flash-boiling multi-hole fuel sprays by employing a Lagrangian methodology based on:

- Implementation of a zero-dimensional flash-boiling atomization model linked to in-nozzle nucleation theory as a boundary condition at the nozzle exit.
- Implementation of an analytical cavitation model to predict effective nozzle diameter at the nozzle exit and comparison with what is expected under flash-boiling conditions.

- Optimization of semi-empirical nucleation model coefficients for use in direct-injection spark-ignition engine simulations under flash boiling spray conditions.
- Investigation of the effect of near-nozzle spray plume expansion through automated modelling adjustment of the initial cone angle at high levels of fuel superheat.

## 2. NUMERICAL METHODOLOGY

The numerical approach is documented in a previous publication of the current authors (Price *et al.*, 2015) however a summary is given here for brevity. A coupled Lagrangian-Eulerian framework was used to enable numerical modelling of a dispersed multi-phase flow. A Lagrangian particle tracking technique was used whereby governing equations (*i.e.* the conservation of mass, momentum and energy) are solved for the individual elements of the dispersed phase (using the stochastic parcel approach where individual droplets are grouped into ‘parcels’ and assumed to have identical physical properties). The continuous phase which is expressed in Eulerian form was solved in the same manner; it incorporates source terms in order to allow for mass, momentum and energy transfer with the dispersed phase, hence a coupled two-phase flow framework. The PISO pressure-velocity coupling algorithm was used (Isaa, 1986) alongside the second-order Monotone Advection and Reconstruction Scheme (MARS), adopted for both momentum and turbulence of the Eulerian phase. Turbulence was modelled using a Reynolds-averaged Navier-Stokes (RANS) approach by employing an eddy viscosity model; specifically the *k*-RNG (Re-Normalization Group) model developed by Yakhot *et al.* (1992) was selected.

The Lagrangian phase was modelled using first-order ordinary differential equations. Mass transfer from surface evaporation was modelled using FORTRAN user subroutines at both subcooled and superheated conditions, which is documented in a previous publication (Price *et al.* 2015), based on the work of Adachi (1996). The Reitz-Diwaker breakup model was adopted to model aerodynamic induced droplet breakup using the default model constants. Droplet-droplet collisions were modelled using the in-built model of STAR-CD based on that of O’Rourke (1992) where a speed-up algorithm has been adopted (Schmidt and Rutland, 2000). The droplet drag model was based on the correlation derived by Schiller and Neumann (1933). This model incorporates two drag coefficients, which relate to a Reynold’s number of less than and greater than  $10^3$  respectively, and is deemed appropriate for evaporating single-component liquid droplets in a gaseous carrier.

Two single-component fuels were investigated, namely *iso*-octane and *n*-pentane, to represent a medium and high volatility component of gasoline, respectively. Temperature dependent polynomial relationships for the thermo-physical properties of those fuels were taken from the Yaws’ Property Database (Yaws, 2003) and implemented via user coding. The fuel properties modelled include: surface tension, viscosity, latent heat of vaporization, density, specific heat capacity, saturation pressure and thermal conductivity. Vapour and gas densities were modelled by the ideal gas law. In the remaining sub-sections important implementations and code development used within the objectives of the current study are documented.

### 2.1 EVAPORATION MODEL

A superheat evaporation model was implemented into the Lagrangian particle tracking framework (Price *et al.*, 2015). A summary is included here for the immediate benefit of the reader. In order to add superheat capability to the code’s framework, a droplet evaporation model was implemented. The mass transfer from the droplet surface is described using two mass transfer terms, namely the subcooled ( $\frac{dM_s}{a}$ ) and superheat terms ( $\frac{dM_{sh}}{a}$ ). The subcooled term is driven by external heat transfer to the droplet surface, and the superheat term is driven by heat transfer from the centre of the

droplet when at superheated conditions. At superheated conditions, the internal droplet temperature is assumed to be constant throughout, and the droplet surface temperature is equal to the fuel boiling temperature at the corresponding ambient pressure. The superheat value  $\Delta T$  is calculated as the difference between the internal droplet temperature and the droplet surface temperature. Once the droplet enters subcooled conditions, the internal droplet temperature and droplet surface temperature are equal. The two terms are as follows (Bird *et al.*, 1966; Spalding, 1953):

$$\frac{dM_s}{d} = A_d P_\infty \frac{Sh D_i}{T_f R_f D_d} \ln \left( \frac{P_\infty - P_v}{P_\infty - P_s} \right) \quad (1)$$

$$\frac{dM_{sh}}{d} = \frac{A_d \alpha \Delta T}{H_L} \quad (2)$$

where  $A_d$  is the droplet surface area,  $P$  the ambient pressure,  $Sh$  the Sherwood number defined as  $Sh = 2 + 0.6 Re^{0.5} Sc^{0.3}$ , where  $Re$  and  $Sc$  are the Reynolds and Schmidt number, respectively,  $D_i$  is the binary diffusivity,  $T_f$  the vapour film temperature,  $R_f$  the vapour film specific gas constant,  $D_d$  the droplet diameter,  $P_v$  and  $P_s$  the partial vapour pressure of the fuel in the computational cell and temperature dependent saturation pressures of the fuel respectively,  $\alpha$  the heat transfer coefficient derived empirically by Adachi *et al.* (1997),  $\Delta T$  the superheat and  $H_L$  the latent heat of evaporation. The empirically defined heat transfer coefficient of Adachi *et al.* (1997) consists of three regimes which occur at varying degrees of superheat, as follows:

$$\begin{aligned} r &= 760 \Delta T^{0.26} \quad \text{when } 0 \leq \Delta T \leq 5 \\ r &= 27 \Delta T^{2.33} \quad \text{when } 5 \leq \Delta T \leq 25 \\ r &= 13800 \Delta T^{0.39} \quad \text{when } \Delta T \geq 25 \end{aligned} \quad (3)$$

The liquid film properties were calculated using the 1/3<sup>rd</sup> rule (Ashgriz, 2011). The total evaporation rate ( $\frac{dM_t}{d}$ ) is calculated as the sum of the subcooled and superheat evaporation terms as:

$$\frac{dM_t}{d} = \frac{dM_s}{d} + \frac{dM_{sh}}{d} \quad (4)$$

The droplet temperature is then calculated by:

$$m C_p \frac{dT_d}{d} = -A_d \alpha (T_d - T) + H_L \left( \frac{dM_t}{d} \right) \quad (5)$$

## 2.2 BOILING POINT AND OTHER PROPERTIES

A boiling point calculation for single component fuels *n*-pentane and *iso*-octane were implemented into the numerical framework to accurately predict the superheat degree in a transient pressure environment, as of that in a running engine. This was completed using the saturation pressure to temperature relationship (Yaws, 2003) of the fuel at a known pressure (the pressure in the cell surrounding the droplet). The saturation pressure polynomial relationship is calculated for *n*-pentane and *iso*-octane respectively as presented in Equation 6 and 7.

$$P_{s,p} = 133.3224 \left( 10^{3.3} \left( \frac{2}{T_d} \right)^{-9.2} - (9.2 \times 10^{-1} T_d) + (9.0 \times 10^{-1} T_d) - (4.1 \times 10^{-6} T_d^2) \right) \quad (6)$$

$$P_{s,i} = 133.3224 \left( 10^{5.3} \left( \frac{3}{T_d} \right)^{-1.1} - (1.1 \times 10^{-1} T_d) + (7.4 \times 10^{-3} T_d) - (9.1 \times 10^{-1} T_d^2) \right) \quad (7)$$

This was compared against boiling temperatures from the NIST database (Brown and Stein) and the Clausius-Clapeyron boiling temperature equation, which calculates the gradient of the vapour pressure curve, displayed in Equation 8:

$$\ln\left(\frac{P_1}{P_2}\right) = \frac{H_L}{R} \left(\frac{1}{T_2} - \frac{1}{T_1}\right) \quad (8)$$

where  $P_2$  and  $P_1$  are known pressures,  $T_2$  is a known boiling temperature at pressure  $P_2$ ,  $T_1$  is the boiling temperature at pressure  $P_1$  and  $R$  is the specific gas constant. The saturation pressure of the fuel followed that of the NIST database and Clausius-Clapeyron relationship closely, with a boiling temperature of 308.1 K and 371.9 K for *n*-pentane and *iso*-octane at 1.0 bar, respectively. The temperature dependency of all other thermophysical properties was taken from Yaws (2003) by implementing suitable correlations (see Price *et al.*, 2015).

## 2.3 NOZZLE EXIT CONDITIONS AND SUB-MODELS

The previous study of the current authors on numerical modelling of flash-boiling fuel sprays from a six-hole injector (Price *et al.*, 2015) is the basis for the model development documented here, whereby the initial droplet diameter was found to be an important parameter when modelling the complex spray structures of flash-boiling. It is well known that superheat is the driving force in flash-boiling, where a larger superheat causes a more severe plume merging and collapsing mechanism in multi-hole injectors. It was found that a smaller initial droplet diameter (as low as ~10% of the nozzle diameter) allowed the code to somewhat predict important characteristics such as spray collapse through air entrainment and droplet-droplet collisions. This reduction in droplet diameter, equivalent to atomization from rapid phase-change, enabled the gaseous phase flow to draw droplets into the central region, promoting spray collapse and plume-plume interactions. A second phenomena promoted by a reduction in droplet diameter and increase in evaporation was droplet recirculation, this is caused by an increase in the velocity magnitude of jet tip vortices as seen by Zhang *et al.* (2013). The reader is referred to (Price *et al.* 2015) for a more in-depth study on these phenomena. In order to add this capability to the code a flash-boiling zero-dimensional atomization model was developed to calculate a suitable boundary condition for the Lagrangian liquid phase.

### 2.3.1 Cavitation Model

The injector under study is associated with cavitation phenomena (Serras-Pereira *et al.*, 2010; Aleiferis *et al.*, 2010; Butcher *et al.*, 2013). Firstly, a cavitation model was used to investigate the in-nozzle phase change phenomena and links with fuel flashing. This study was carried out using the model developed by Sarre *et al.* (1999), whereby the saturation pressure is used along with a contraction ratio and fuel properties to predict the reduction in effective nozzle diameter. This model could be particularly suited to flash-boiling applications due to the effect of temperature being considered through the temperature dependent saturation pressure. The following procedure was used to calculate the reduction factor caused by cavitation. Firstly, the pressure at the vena contracta,  $P_{vena}$  is calculated:

$$P_v = P_i - \frac{\rho_l}{2} U_v^2 \quad (9)$$

where  $P_i$  is the upstream injection pressure and  $U_v$  the velocity on the central axis of the nozzle at the vena contracta, calculated as follows:

$$U_v = \frac{U_m}{C_c} \quad (10)$$

where  $U_{mean}$  is the mean liquid velocity in the nozzle and  $C_c$  the contraction ratio.  $U_{mean}$  is calculated by Equation 11:

$$U_m = \frac{\dot{m}}{A_n \rho_l} \quad (11)$$

where  $\dot{m}$  is the mass flow rate and  $A_n$  the nozzle hole area. It should be noted that the droplet velocity profile is considered constant here. The contraction ratio,  $C_c$  can be calculated via the following formula originally devised by (Nurick, 1976):

$$C_c = \left[ \left( \frac{1}{C_c} \right)^2 - 11.4 \left( \frac{r}{D} \right) \right]^{-0.5} \quad (12)$$

where  $C_{co}$  is derived from experimental data at known values of  $C_c$  and  $r/D$  (roundness ratio at the nozzle hole inlet) and is calculated as 0.61 (Sarre *et al.*, 1999).

The effective velocity,  $U_{eff}$  at the nozzle orifice can now be calculated:

$$U_e = \frac{A_n}{\dot{m}} (P_s - P_\infty) + U_v \quad (13)$$

where  $P$  is the ambient pressure downstream of the nozzle. From the effective velocity the effective nozzle geometry can be calculated as:

$$D_e = \sqrt{\frac{4\dot{m}}{\pi U_e \rho_l}} \quad (14)$$

Where  $A_{eff}$  and  $D_{eff}$  are the effective nozzle area and diameter, respectively. This reduction in geometry can be translated to a reduction factor caused by cavitation:

$$R_{d,c} = \frac{D_e}{D} \quad (15)$$

A number of parameters are required for the application of this model to various types of fuel injectors and not much work has been done along those lines specifically for spark-ignition engine fuels that have much higher volatility than diesel. The spark-ignition engine injector and conditions under study here relate to 0.2 mm nozzle diameter and 150 bar injection pressure, leading to typical nozzle Reynolds numbers of about 30,000 and 50,000 at 293 K, 1 bar (Aleiferis and van Romunde, 2013), depending on fuel type. The  $r/D$  ratio was estimated at ~0.05–0.1 from the electron microscope images of Butcher *et al.* (2013, 2015). This value is situated within the range suggested of 0.01–0.08 being equivalent to sharp and rounded injector radii, respectively. For  $r/D$  of 0.05,  $C_c$  would be 0.678.

The discharge coefficient is calculated for a range of  $L/D$  ratios which were compared to experimental results from (Lichtarowicz *et al.*, 1965). This is displayed in Figure 2. The  $L/D$  ratio of the injector under study was approximately 1.0–1.1 (depending on hole orientation) (Butcher *et al.*, 2013, 2015). A good trend is displayed for the discharge coefficient of the cavitation model, with the majority of analytical data points lying within the range of experimental data. The short  $L/D$  ratio of 1.1 resides close to the outer range of the validation case, where the discharge coefficient becomes very sensitive to  $L/D$  and can drop significantly. It is noted that, although a value of

$\sim 0.809$  was calculated from Figure 2 for  $L/D=1.1$ , the current injection system has been characterised to have a discharge coefficient of  $\sim 0.6$  (Butcher *et al.*, 2013). This confirms the sensitivity displayed in Figure 1 when one goes so close to  $L/D$  unity.

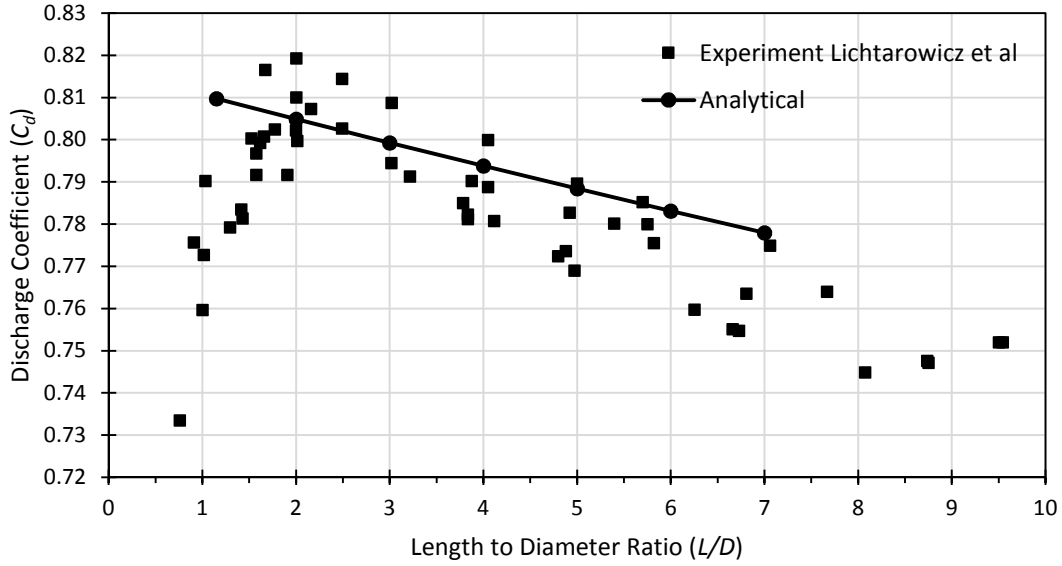


**Figure 1:** Validation of cavitation model by comparison of discharge coefficient with experimental data (Lichtarowicz *et al.* 1965).

The discharge coefficient and contraction ratio can be linked through the following equation (Nurick, 1976):

$$C_d = C_c \sqrt{\frac{P_i - P_s}{P_i - P_\infty}} \quad (16)$$

Both the analytical calculation (0.809) and experimental discharge coefficient of Butcher *et al.* (2013) (0.6) were used to calculate the equivalent contraction coefficient and subsequent droplet reduction factor, as shown in Figure 2.

The reduction from cavitation can be seen for both *n*-pentane and *iso*-octane at varying fuel temperatures and ambient pressures using both  $C_c=0.809$  and  $C_c=0.6$ . It is clear that the effect of ambient pressure on cavitation is minimal, due to the overall pressure differential between injection pressure ( $P_i$ ) and downstream ambient pressure ( $P$ ) varying from  $\Delta P=150.0-1.0=149.0$  bar to  $\Delta P=150.0-0.5=149.5$  bar, a small relative increase. In the current application the effect of fuel temperature on cavitation is important and is taken into account through the temperature dependent saturation pressure curve, resulting in an increase in cavitation for higher fuel temperature conditions. The prediction of a higher degree of cavitation for *n*-pentane compared to *iso*-octane is a result of the high and low fuel volatilities respectively. However, the cavitation model seems to under-predict the degree of phase change from thermal mechanisms with respect to previous studies into the required initial droplet diameter at the nozzle exit for spray collapse to be induced (Price *et al.*, 2015). Due to this under-prediction it is clear that the analytical cavitation model on its own is not really suitable at high levels of vapour pressure from superheats. Therefore, it was decided to look further into other types of sub-modelling that would involve explicitly the mechanism of nucleation at superheated conditions. Therefore two nucleation models, originally developed for superheated liquids in pipe/nozzle flows, were implemented and compared, as discussed in the next sections.

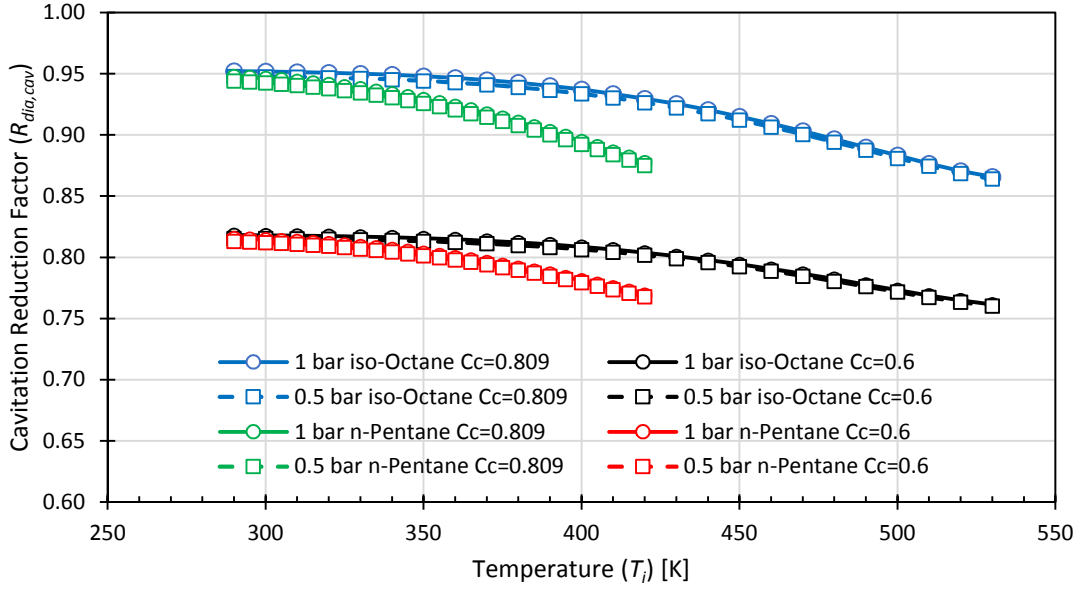


**Figure 2:** The reduction factor predicted from cavitation effects with varying temperature and pressure for both *n*-pentane and *iso*-octane fuels.

### 2.3.2 Nucleation Model 1

The first model was based on the wall nucleation study published by Riznic and Ishii (1989). Riznic and Ishii (1989) found that the original model developed for pool and convective boiling could be appropriately modified via a superheat term for the application in flashing pipe flows, whereby validation was carried out in cylindrical tubes with a diameter of 20 mm. The model fundamentally relies on three parameters, namely the nucleation site density, bubble departure diameter and the departure frequency. The model is implemented into the code as follows:

Firstly, nucleation site density per unit surface is calculated based on a dimensionless nucleation site density function as well as a property function dependent on the liquid to gas density ratio as displayed in Equation 17:

$$N_n = \frac{1}{D_b^2} N_n^* F(\rho^*) \quad (17)$$

where the dimensionless nucleation density,  $N_n^*$  is given as:

$$N_n^* = \left( \frac{2\sigma T_s}{D_b(T_l - T_s)\rho_g H_L} \right)^{-4.4} \quad (18)$$

Here  $\sigma$  is the surface tension coefficient,  $T_{sat}$  the saturation temperature of the fuel,  $D_b$  the bubble departure diameter,  $T_l$  the fuel temperature,  $\rho_g$  the fuel vapour density and  $H_L$  the latent heat of vaporisation. Secondly, the bubble departure diameter is calculated as follows:

$$D_b = 2.64 \times 10^{-5} \theta \left( \frac{\sigma}{g\Delta\rho} \right)^{0.5} (\rho^*)^{0.9} \quad (19)$$

where  $\theta$  is the contact angle,  $\sigma$  the surface tension,  $g$  the acceleration due to gravity,  $\Delta\rho$  the dimensional density ratio and  $F(\rho^*)$  the property density function. The contact angle can be set typically to a value of  $45.78^\circ$ , as previously adopted by Janet *et al.* (2015).

The property density function and dimensionless density are defined in Equation 20 and 21, respectively.

$$F(\rho^*) = 2.157 \times 10^{-7} (\rho^*)^{-3.1} (1 + 0.0049 \rho^*)^{4.1} \quad (20)$$

$$\rho^* = \frac{\rho_l - \rho_g}{\rho_g} \quad (21)$$

where  $\rho_l$  is the liquid density. It is clear that the density of the fuel has a direct effect on the nucleation site density, where a reduction in the dimensionless density causes an increase in nucleation site density. Finally the bubble departure frequency is calculated as follows:

$$f = \frac{1.18}{D_b} \left( \frac{\sigma (\rho_l - \rho_g)}{\rho_l^2} \right)^{0.2} \quad (22)$$

### 2.3.3 Nucleation Model 2

The second model employed is documented by Janet *et al.* (2015) where multiple existing models are combined. Firstly, the model calculates the nucleation site density taken from Lemmert and Chawla (1977). Two reference values are required namely,  $N_{ref}$  which is defaulted as  $7.937 \times 10^5 \text{ m}^{-2}$  and,  $\Delta T_{ref,1}$  defaulted as 10 K. The nucleation site density is also a direct function of superheat, as displayed in Equation 23:

$$N_n = N_r \frac{T_l - T_s}{\Delta T_{r,1}} \quad (23)$$

Secondly, the bubble departure diameter taken from Kurul and Podowski (1991) is also calculated via reference parameters;  $D_{ref}$ ,  $D_{max}$  and  $\Delta T_{ref,2}$  which are suggested as  $6 \times 10^{-4} \text{ m}$ ,  $1.4 \times 10^{-3} \text{ m}$  and 45 K, respectively. However, due to a smaller nozzle diameter in the current work (0.2 mm), alternative values are adopted based on the volumetric flow rates predicted and specific nozzle geometry, which are shown in Table 1. The calculation for bubble departure diameter is displayed in Equation 24:

$$D_b = \max \left( D_r \exp \left( \frac{T_l - T_s}{\Delta T_{r,2}} \right), D_m \right) \quad (24)$$

The frequency is calculated based on the equation developed by Cole (1967) where velocity and bubble departure diameter are employed:

$$f = \sqrt{\frac{4g(\rho_l - \rho_g)}{3C_d D_b \rho_l}} \quad (25)$$

The nucleation models documents can be used to predict a volumetric flow rate of vapour caused by in-nozzle phase change which is documented in the following section.

**Table 1:** Values adopted for model 2 (Lemmert and Chawla, 1977; Kurul and Podowski, 1991).

Reference Parameter	Value
$N_{ref}$	$7.937 \cdot 10^5 \text{ m}^{-2}$
$\Delta T_{ref,1}$	10 K
$D_{ref}$	$4 \cdot 10^{-5} \text{ m}$
$D_{max}$	$1 \cdot 10^{-5} \text{ m}$
$\Delta T_{ref,2}$	50 K

It is worth mentioning that the nucleation model derived by Blinkov *et al.* (1993) and documented in the work of Janet *et al.* (2015) was not adopted in the current work. The authors decided to not include this approach due to its empiricism and lack of specific case variables, but it may offer a more suitable approach to some specific applications closer to the original study.

### 2.3.4 Diameter Reduction Factor

The requirement for a primary atomization model and subsequent boundary condition for the Lagrangian liquid phase at flash-boiling conditions is predicted from the aforementioned nucleation models which take into account injection pressure, fuel temperature, fuel properties and nozzle geometry. To predict the reduction in initial droplet diameter being discharged from the nozzle orifice, as previously documented in (Price *et al.*, 2015), the following process was carried out.

The volumetric flow rate was calculated using the nucleation site density, wall departure bubble volume, departure frequency and in-nozzle surface area,  $S_{nozzle}$  as follows:

$$\dot{V}_v = N_n V_{bf} S_n \quad (26)$$

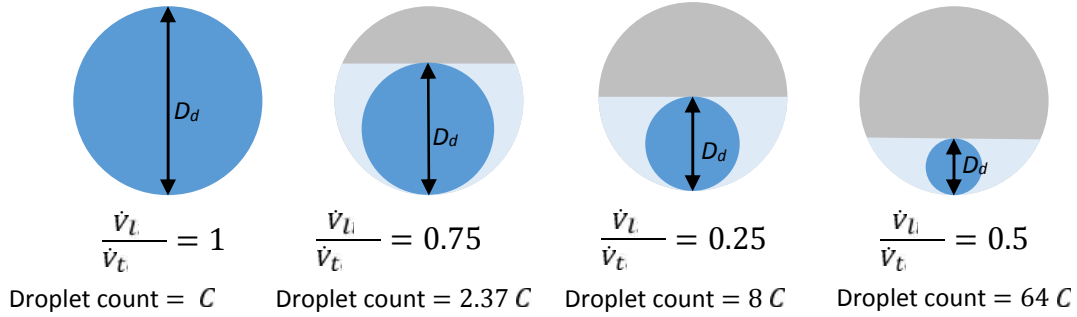
Using this prediction of vapour volume flow rate, the void fraction can be calculated based on the transfer of mass through phase change from liquid to vapour and the volumetric fractions of each phase. A constant mass flow rate is adopted in the current work and hence a fuel and condition specific volumetric flow rate is used in the calculation of in-nozzle vapour void fraction. In order to implement the reduction in initial droplet diameter to the code through user-coded subroutines, a reduction factor was derived from the degree of phase change predicted from the nucleation model, assuming a homogenous distribution of vapour bubbles at the nozzle exit and a direct dependency on the liquid to total volume flow rate. The ratio of liquid volume flow rate and total volume flow rate is used as displayed in Equation 27:

$$\frac{\dot{V}_t - \dot{V}_v}{\dot{V}_t} = \frac{\dot{V}_{li}}{\dot{V}_t} \quad (27)$$

This is purely a scaling factor and represents a limit to the maximum possible droplet diameter leaving the nozzle exit, and one does not assume a single droplet is present. The conservation of mass is achieved computationally through increasing the parcel count (representing multiple droplets exiting the nozzle), accounting for the reduced droplet mass of the smaller droplets, and henceforth obeying continuity. A schematic is displayed in Figure 3 demonstrating the approach used (asymmetric vapour film leading to ‘wall droplets’) as well as an alternative approach (symmetric vapour film) to limit droplet diameter based on the percentage of liquid in the nozzle.

## Atomization and Sprays

### Asymmetric Vapour Film



### Symmetric Vapour Film

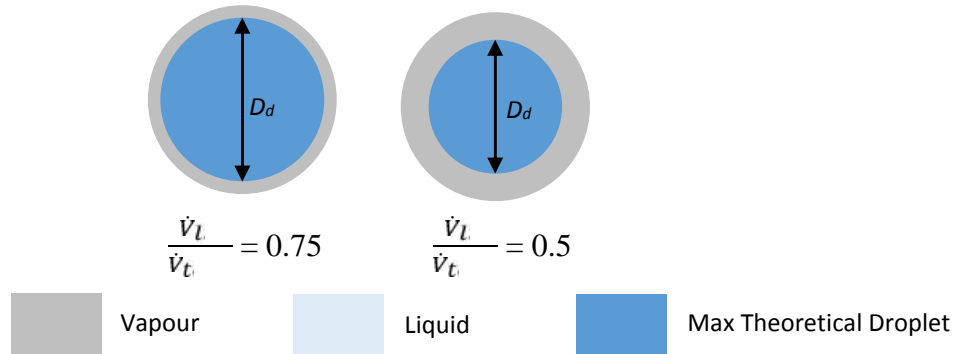


**Figure 3:** A schematic showing the initial droplet diameter reduction factor.

It can be seen that the theoretical diameter limit is achieved through scaling from the ratio of  $\dot{V}_L$  to  $\dot{V}_t$ . The liquid displayed in Figure 3 is accounted for by increasing the droplet count of the stochastic parcel, which is displayed as a function of  $C$  which corresponds to the droplet count of a parcel containing droplets the size of the nozzle orifice. The second approach to translating the phase change to a droplet diameter was also studied, whereby a vapour film surrounds a spherical droplet. It is clear that one can adopt several methodologies in deriving an effective droplet diameter. In the current work the asymmetric vapour film methodology has been adopted, due to it representing the asymmetric nature of a working injector, whereby the upper surface is usually subject to cavitation and thermal effects as well the influence of mechanically driven flow towards the lower portion of the nozzle (see optical nozzle studies like those of Serras-Pereira *et al.*, 2010 and Aleiferis *et al.* 2010).

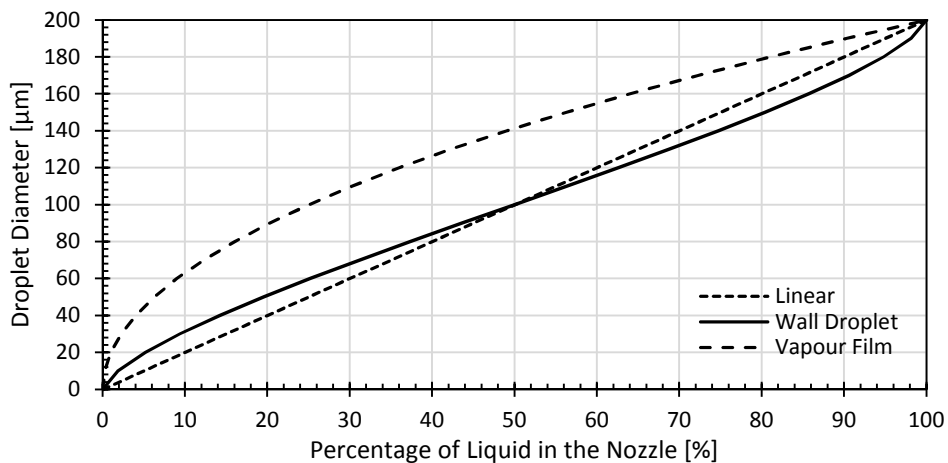


**Figure 4:** A graph showing the difference between three translation techniques to quantify an effective droplet diameter with varying percentage of liquid in the nozzle.

The difference between each approach (including a basic linear relationship) is displayed in Figure 4, and the influence of this on the application of the proposed model is mentioned in section 5. It should be noted that this is an initial step in using bubble nucleation theory to provide a primary atomization model in the case of an Eulerian/Lagrangian framework, where a number of assumptions currently exist. These assumptions include: evenly distributed nucleation sites and bubble departure in the bulk fluid over the entire inner surface of the nozzle orifice, a single constant departure diameter, spherical bubbles and a homogenous distribution of bubbles throughout the bulk fluid. The mass flow rate is kept constant despite only the liquid phase being modelled in the Lagrangian framework, this assumption was based on calculations of the mass lost as vapour inside of the nozzle being approximately 0.05% at  $T_i=450$  K and  $P = 1$  bar for *n*-pentane fuel. Further effects of bubble growth were not implemented in the primary atomization model, as the assumption that a constant bubble departure diameter evenly distributed over the entire in-nozzle area was used, which means the bubble diameter is the mean diameter (representing bubbles at the nozzle mid-point) and hence the effects of bubble growth are not determined. This was considered an acceptable approach within the bounds of the current paper as little effect is seen on the subsequent droplet diameters with the above assumptions.

### 3. SIMULATION SET-UP

A typical multi-hole gasoline injector geometry was used. This consisted of 6 nozzle orifices of 0.2 mm diameter each and a nominal spray plume cone angle of  $15^\circ$  at 293 K, 1 bar. An extensive experimental database exists on this specific injector, at a wide range of operating conditions and fuels, obtained from optical experiments (*e.g.* van Romunde *et al.*, 2007; Aleiferis and van Romunde, 2013; Serras-Pereira *et al.*, 2007, 2008, 2015); further geometrical information can be found within these previous publications. Table 2 displays all spray conditions simulated in the current work whereby the Jakob number has been used to compare each spray case through non-dimensionality and the calculated values are in the range found in literature for highly flash-boiling sprays (Shepherd and Sturtevant, 1982). The Jakob number was calculated as follows:

$$J_t = \frac{c_p(\Delta T)\rho_L}{H_L\rho_g} \quad (28)$$

All comparisons between simulations and experimental spray shadowgraphs are made at a time of 777  $\mu$ s after start of injection (ASOI), unless otherwise stated. The mass flow rate was taken from the measurements of Serras-Pereira *et al.*, (2010) and Butcher *et al.*, (2013). A temperature-dependent velocity calculation was implemented, with velocities ranging from  $\sim 90$ – $165$  m/s for fuel temperatures in the range  $20^\circ$  C to  $180^\circ$  C. The current study was based on previous characterisation of the injector operating at  $P_i=150$  bar injection pressure.

The spray simulations were carried out in an initially quiescent chamber of dry air at  $20^\circ$  C discretized in a cubic domain of 512,000 cells of 1-mm nominal size. A grid dependency study was carried out whereby a range of cells were studied, namely 0.5, 1, 2 and 3 mm. The results of this study have been documented in Price *et al.* (2015). A time step of 1  $\mu$ s was employed according to the requirement for future implementation into engine simulations; to put this number into perspective, it is noted that 1 crank angle degree at 1500 RPM corresponds to 111  $\mu$ s.

**Table 2:** Spray conditions documented with respect to the dimensionless Jakob number.

Fuel	Temperature ( $T_i$ ) [K]	Ambient Pressure ( $P$ ) [bar]	Superheat ( $T$ ) [K]	Jakob Number ( $Ja$ )
<i>n</i> -Pentane	363	0.5	77	428.22
<i>n</i> -Pentane	393	1.0	84.9	203.43
<i>n</i> -Pentane	393	0.5	104	500.61
<i>n</i> -Pentane	453	0.3	176.1	671.30
<i>iso</i> -Octane	453	0.3	117.9	589.20

## 4. RESULTS AND DISCUSSION

### 4.1 SUBCOOLED SPRAY FORMATION

Firstly the current computational framework was validated at subcooled conditions, namely  $P = 1$  bar and  $T_l = 293$  K. Displayed in Figure 5 is a comparison between an *iso*-octane spray simulation at subcooled conditions with experimental shadowgraph images 777  $\mu$ s ASOI. A schematic of the injector orientation has also been included for additional clarity.

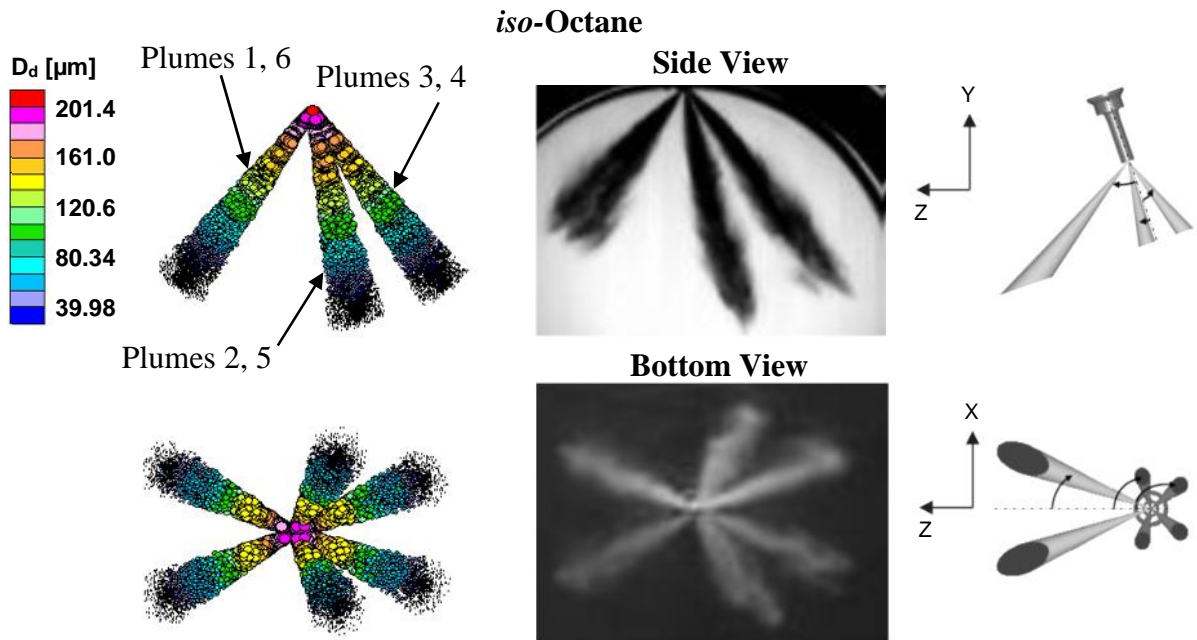


**Figure 5:** Computational and experimental *iso*-octane spray images at  $P = 1$  bar and  $T_l = 293$  K.

The computational spray characteristics represent the experimentally observed characteristics quite accurately. To quantitatively validate the current numerical framework, liquid penetrations were measured for plumes 1 and 6 for both *iso*-octane and *n*-pentane simulations and compared to experimental data as displayed in Figure 6. The penetration is predicted within  $\sim 5\%$  and  $\sim 1\%$  for *n*-pentane and *iso*-octane respectively at 1000  $\mu$ s ASOI. Note that the experimental injection delay has been incorporated by delaying the computational start of injection (SOI) by 315  $\mu$ s (van Romunde and Aleiferis 2009).

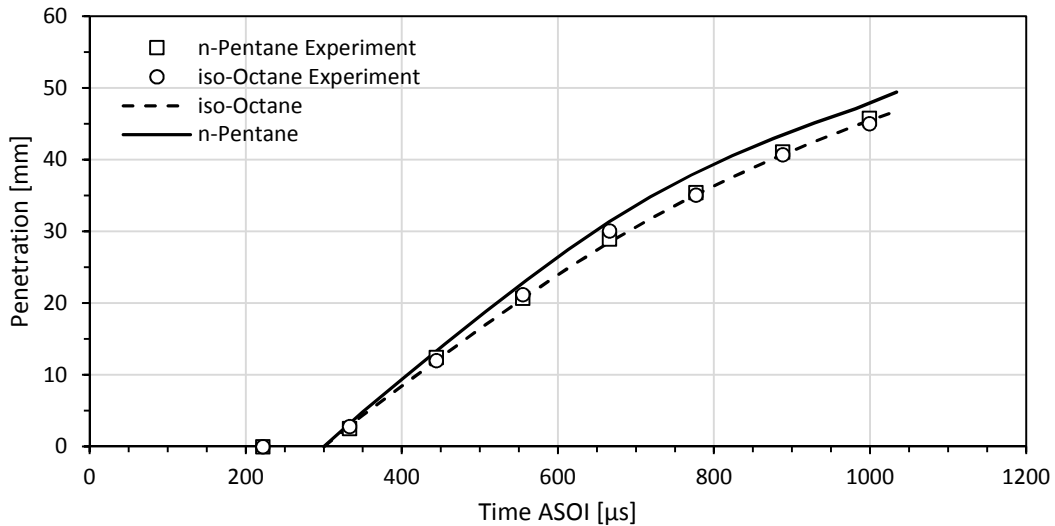


**Figure 6:** Liquid penetration for  $n$ -pentane and  $iso$ -octane at  $P = 1$  bar and  $T_l = 293$  K.

## 4.2 SUPERHEATED ATOMIZATION

The numerical framework of Price *et al.* (2015) was able to predict important flash-boiling spray characteristics using an initial parametric study. Hereon the aim of the current work was to automatically predict suitable and appropriate Lagrangian spray boundary conditions with respect to fuel properties and operating conditions.

Firstly, the volumetric flow rate of vapour produced from heterogeneous wall nucleation of both  $n$ -pentane and  $iso$ -octane fuels was calculated and a comparison between both models is made. Here an ambient pressure of  $P = 1.0$  bar is used for the purposes of clarity. The predicted volumetric flow rate is displayed in Figure 7.

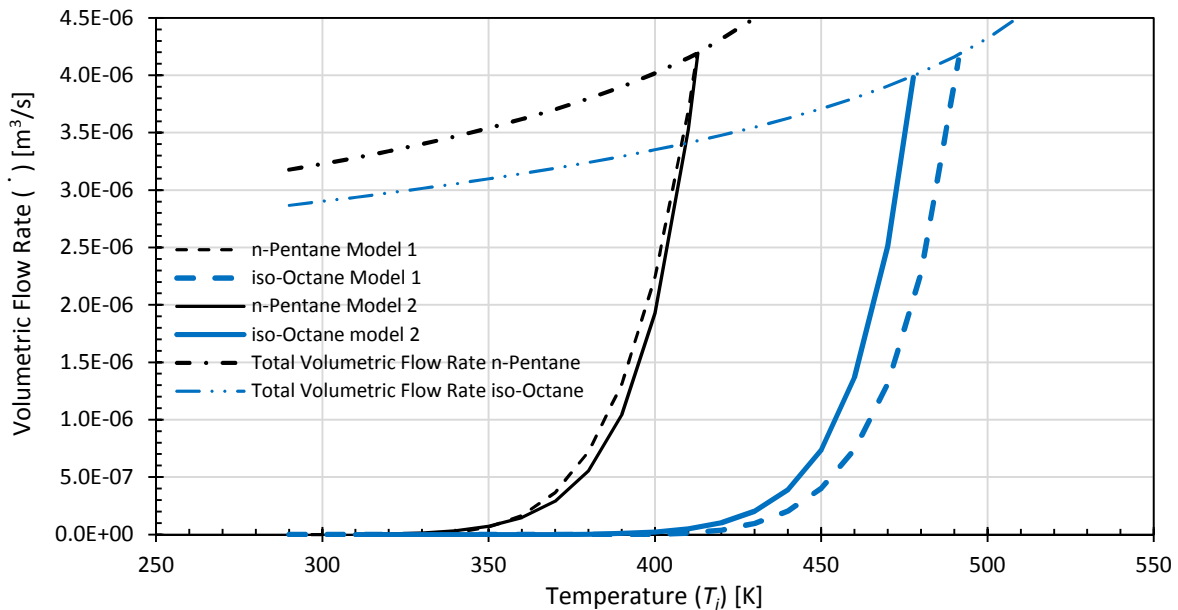


**Figure 7:** Volumetric flow rate of vapour for  $n$ -pentane and  $iso$ -octane using model 1 and model 2.

It can be seen that the prediction of in-nozzle vapour is heavily dependent on superheat degree, specifically at high temperatures where the superheat exceeds  $\Delta T = 90$  K. The total volumetric flow rate is also plotted to allow the magnitude of predicted volume to be clearly understood. The effect of volumetric flow rate of vapour on the mass flow rate of liquid being injected was investigated and the change in injected mass was small for temperatures higher than 293 K ( $\sim 0.05\%$  at 450 K),

hence the nominal mass flow rate at 293 K was used even at high superheat degrees. The degree of superheat needed for the vapour volumetric flow rate to equal 50% of the total volumetric flow rate was approximately  $\Delta T=90$  K for both *n*-pentane and *iso*-octane fuels. Model 1 predicts a smaller volumetric flow rate of vapour for *iso*-octane, resulting in a superheat of  $\Delta T \sim 100$  K for a 50% vapour to total volumetric flow rate.

The two nucleation models adopted here predict vapour volumetric flow rates within approximately 5% and 40% for *n*-pentane and *iso*-octane at  $T_i=363$  K and  $T_i=453$  K, respectively. The difference seen in the case of *iso*-octane is caused by the constant reference values used in model 2 which may not be a suitable approach for a fairly significant variation in fuel properties, specifically the large variation in volatility. The approach of model 1 is less dependent on empirical variables, and may be more suitable to this application where large variations in fuel properties are a frequent occurrence. Using the volumetric flow rate of vapour and the total volumetric flow rate, the volume void fraction in the nozzle was predicted using Equation 27. Here the void fraction was calculated from the predicted volume of vapour residing in the nozzle orifice, which is assumed to be occupied entirely by liquid fuel apart from the liquid to vapour phase change associated with bubble nucleation. Here the void fraction corresponds to the volume void fraction, based on the aforementioned adopted assumptions. The volume void fraction was then directly translated as the boundary condition for the initial droplet diameter at the nozzle orifice.

The droplet diameter reduction factor is displayed in Figure 8 along with a schematic diagram associated with 0, 0.5 and 0.75 void fraction. The schematics represent the approach of the atomization model applied to the Lagrangian spray framework.

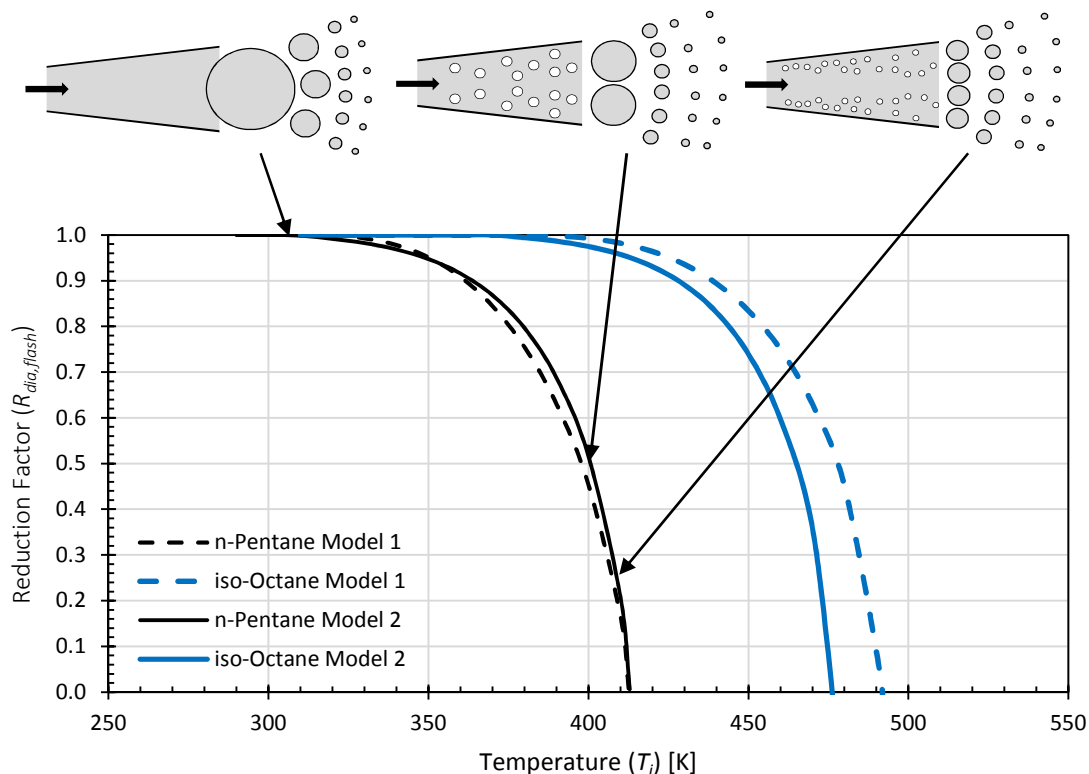


**Figure 8:** Droplet diameter reduction factor for *n*-pentane and *iso*-octane for model 1 and model 2.

Also shown are three schematic diagrams associated with a reduction factor of 1, 0.5 and 0.25.

At low temperatures, the droplet diameter leaving the nozzle orifice corresponds to the ‘blob’ method, which assumes the droplet is equal to the nozzle diameter and subsequently goes through

significant aerodynamic induced break-up resulting in an atomised spray downstream of the nozzle. The centre and right schematic diagrams correspond to a void fraction of 0.5 and 0.75 respectively, where the initial droplets are estimated to be half and quarter of the nozzle diameter. Note that the number of droplets will increase to satisfy continuity. The smaller initial droplets will subsequently go through a similar, more limited aerodynamic induced break-up phase. The reduced droplet size corresponds to experimental studies whereby optical nozzles are used to quantify in-nozzle flashing mechanisms such as nucleation and droplet formation (Park and Lee 1994; Zhang *et al.* 2015). The subsequent reduction in droplet size and the under-expanded nature of the now two-phase flow promote air entrainment, in turn promoting spray collapse.

In order to validate the zero-dimensional atomization model, both the bubble number density and void fraction of vapour of model 1 are compared to optical experimental data of Li *et al.* (2015). The bubble number density is compared in Figure 9 at a range of superheats, which in this case is characterised by the ratio of  $P$  and  $P_s$ . To directly compare bubble number density calculations to experimental data, ethanol fuel was implemented into the model. Due to surface nucleation being the mechanism modelled in the zero-dimensional atomization model, the authors believe that a direct comparison can be made to the experimental study. Whereby a 2D ‘slit’ nozzle was used and explicitly defined as a single layer of bubbles with no overlapping, hence bubble number density per surface area is comparable.

It is clear that the bubble number density for ethanol lies within the range seen in experiment. Through normalising the fuels via superheat degree, it can be concluded that superheat degree is the dominant parameter whereby all fuels lie within a small range typically in the order of  $10\text{--}30\text{ mm}^{-2}$  at a superheat of  $\frac{P_\infty}{P_s}=0.1$ . To validate the model as a whole, the vapour percentage of the nozzle orifice is used to compare to experimental data. The void corresponds to the ratio of vapour to total area on a 2D plane perpendicular to the nozzle axis. The fraction of vapour to liquid is taken as defined in Equation 27. The subsequent values of void fraction at varying superheat degrees are displayed in Figure 10.

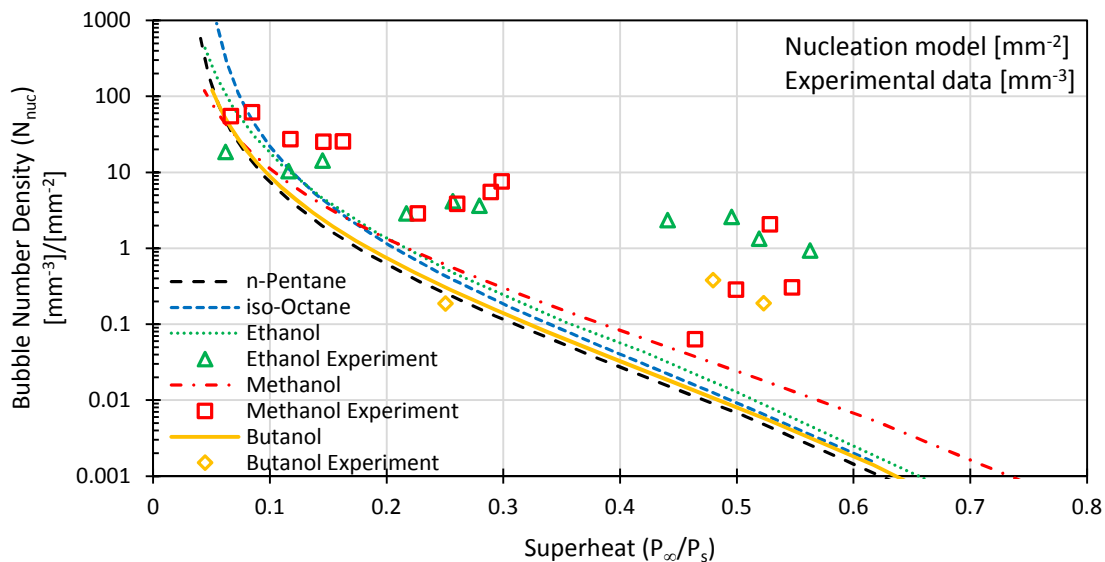


**Figure 9.** Comparison of predicted bubble number density with varying superheat degree to experimental data of Li *et al.* (2015) using *n*-pentane, *iso*-octane and alcohols at  $P = 1$  bar.

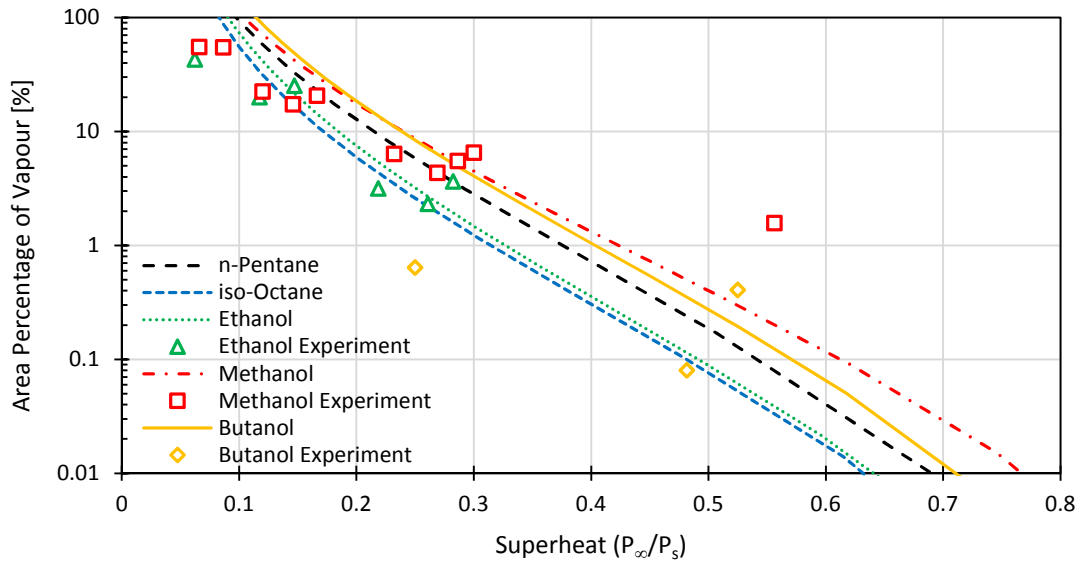


**Figure 10:** Comparison of predicted in-nozzle area fraction of vapour with varying superheat degree to experimental data of Li *et al.* (2015) using *n*-pentane, *iso*-octane and alcohols at  $P = 1$  bar.

The predicted void fraction of vapour in the nozzle lies close to experimental data for all fuels, whereby the analytical model predicts very similar void fractions when normalised through superheat, with the differences stemming from fuel properties such as density and latent heat of evaporation. Considering the well documented difficulty in predicting nucleation (Girshick and Chiu, 1990) the code’s ability to match experimental data gives confidence in the modelling approach.

To further study the capability of the flash-boiling atomization model the effect of downstream ambient pressure,  $P$  is studied. Displayed in Figure 11 and Figure 12 are the predicted initial droplet diameters by the two atomization models respectively, at ambient pressures of  $P = 1.0$  bar,  $P = 0.5$  bar and  $P = 0.3$  bar. The dominant pressure dependent variables here are fuel vapour density,  $\rho_g$  and saturation temperature  $T_{sat}$  which increase nucleation as ambient pressure reduces.

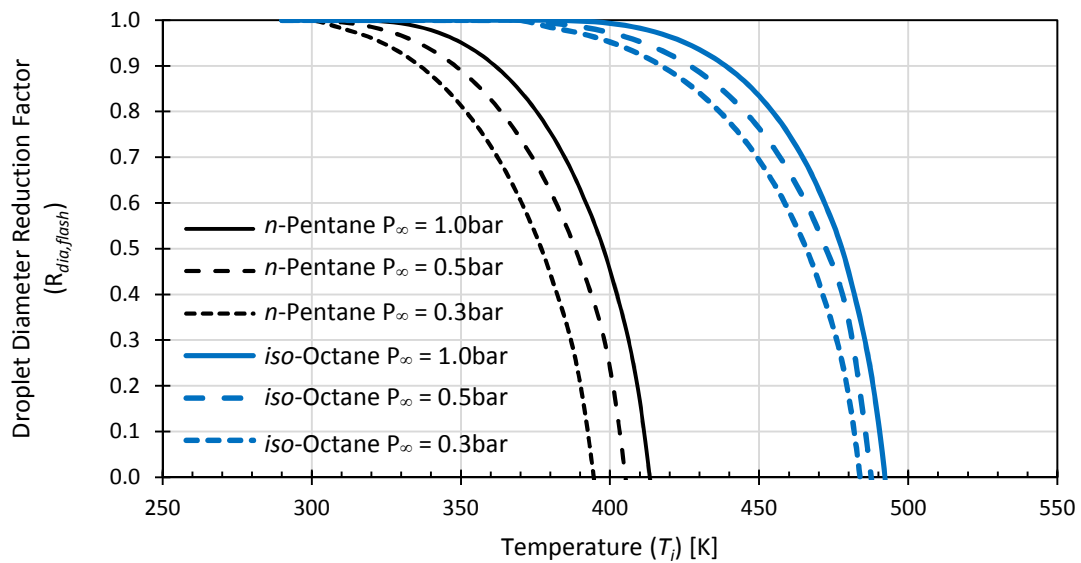


**Figure 11:** The predicted droplet diameter at varying temperature for model 1 at ambient pressures of  $P = 1.0$  bar,  $P = 0.5$  bar and  $P = 0.3$  bar.

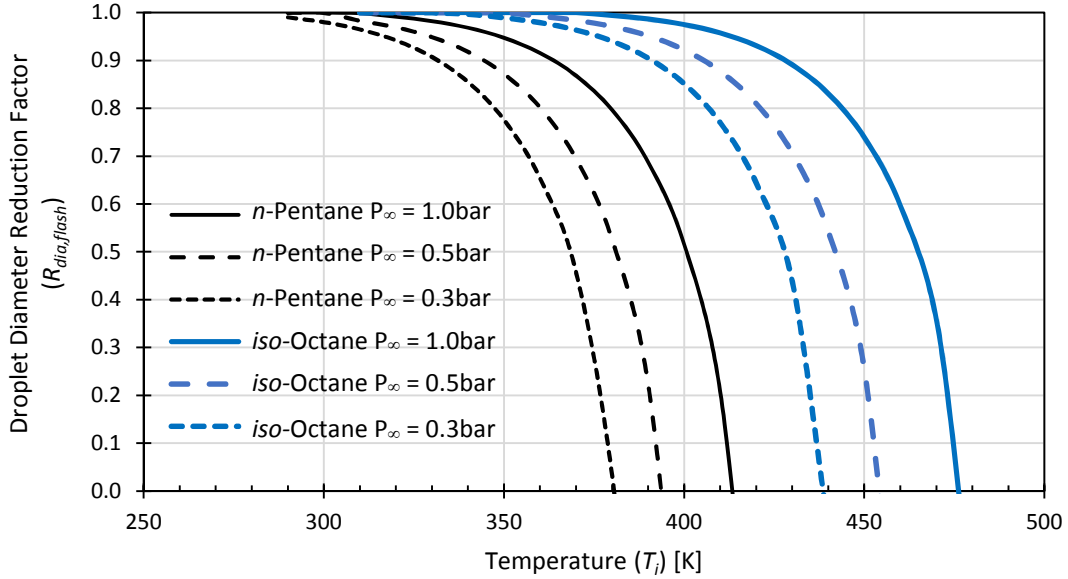


**Figure 12:** The predicted droplet diameter at varying temperature for model 2 at ambient pressures of  $P = 1.0$  bar,  $P = 0.5$  bar and  $P = 0.3$  bar.

It can be seen that reducing the ambient pressure reduces the predicted initial droplet diameter at a given temperature, and becomes more significant at high superheats due to the exponential nature of nucleation. Focusing on model 1, at  $T_l = 333$  K the predicted droplet diameters for *n*-pentane are  $D_d = 199.9 \mu\text{m}$ ,  $197.08 \mu\text{m}$  and  $191.66 \mu\text{m}$  for  $P = 1.0$  bar,  $P = 0.5$  bar and  $P = 0.3$  bar respectively, a maximum reduction of 4.17%. However, at higher temperatures where the model is more sensitive to temperature change the predicted droplet diameters become significantly smaller. At  $T_l = 363$  K the calculated initial droplet diameters are  $D_d = 187.2 \mu\text{m}$ ,  $169.7 \mu\text{m}$  and  $143.0 \mu\text{m}$  respectively, a 23.33% reduction from  $P = 1.0$  bar to  $P = 0.3$  bar. Model 2 gives the same trend, however the effect of pressure is more substantial with a maximum reduction in droplet size from  $P = 1.0$  bar to  $P = 0.3$  bar ambient pressure of 38.36% at  $T_l = 363$  K.

In summary, the flash-boiling atomization model implemented gave reasonable trends for the prediction of a reducing initial droplet diameter with superheat degree. The current reference values used as empirical coefficients do not give optimum predictions of initial droplet diameter based upon the conclusions from the previous parametric study of the current authors (Price *et al*, 2015), and a ‘model refinement’ section is documented subsequently. Here the potential to tweak model coefficients to improve predicted spray characteristics in terms of liquid penetration and spray structure was investigated. From here on, model 1 is selected for further development due to its dimensionless nature as well as its more empirically independent manner.

## 5. MODEL REFINEMENT AND DISCUSSION

The primary atomization model does not predict the optimum droplet diameters for the computation of a collapsing spray at various fuel temperatures and ambient pressures when modelled in the current framework using the default parameters. However, it does produce a promising methodology for predicting flash-boiling spray characteristics using a Lagrangian Particle Tracking method based on nucleation physics. This section attempts to improve the model's prediction in the context of the current injection system set-up, by varying a semi-empirical model parameter which is used to characterise the boiling surface (Kocamustafaogullari and Ishii, 1983). The exponent,  $y$ , of the dimensionless nucleation site density term is varied as shown in Equation 29.

$$N_n = \frac{1}{D_d^2} \left( \frac{2\sigma l_s}{D_d \rho_g (T_l - T_s) \Delta H_L} \right)^{-y} F(\rho^*) \quad (29)$$

This exponent is a suitable parameter for model optimisation due to the dimensionless nature of the term and its function of characterising the boiling surface. Due to the obvious constraints in measuring accurately the surface features, this parameter can understandably offer improvement for correlation with experimental data, as stated by Kocamustafaogullari and Ishii (1983). The effect of varying this parameter, on the subsequent initial droplet diameter reduction factor, from its default value of 4.4 to 4.5195 and 4.6 at  $P = 1.0$  bar is displayed in Figure 13.

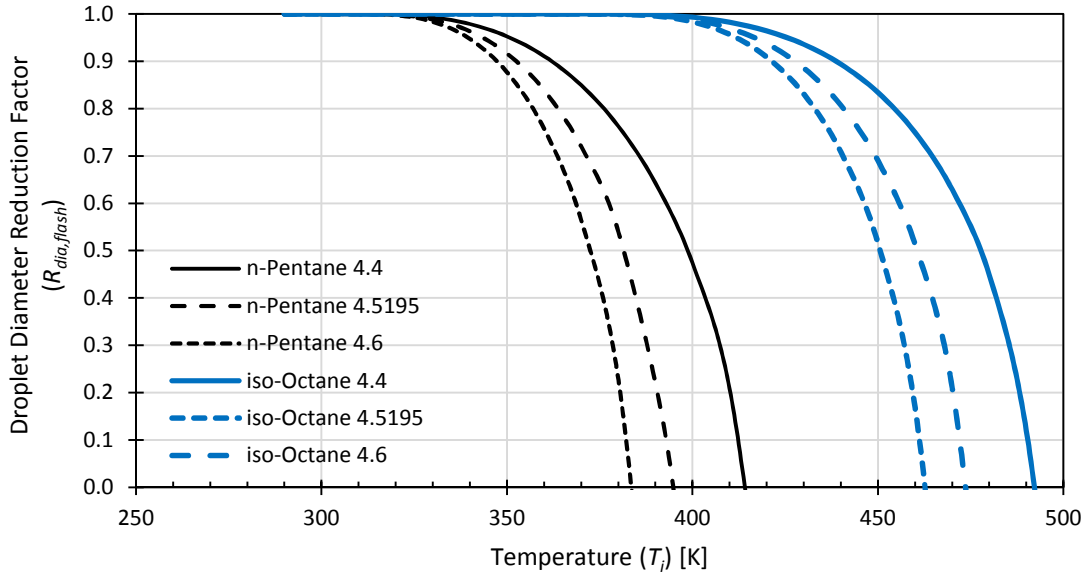


**Figure 13:** Droplet diameter reduction factor with varying temperature at  $P = 1.0$  bar; plotted using exponent values of 4.4, 4.5195 and 4.6 for both *n*-pentane and *iso*-octane.

The exponent value of 4.5195 was chosen due to prediction of initial droplet size for *n*-pentane at  $T_f = 393$  K and  $P = 1.0$  bar ( $D_d = 18.8$   $\mu\text{m}$ ) that generally matched the observations of the previous parametric study of Price *et al.* (2015). The value of 4.6 was also plotted to give the authors a wider range of influence from the changing nucleation site density. It can be seen that the model is very sensitive to the exponent,  $y$  varying the reduction factor significantly at high fuel temperatures. This allowed the model to be modified to predict reasonable droplet diameters at  $P = 1.0$  bar ambient pressure conditions, predicting flash-boiling spray characteristics which are discussed below. It is worth noting here that one would need to use a value of  $y = 4.513$  and  $y = 4.5245$  to reach the equivalent reduction factor for the linear and vapour film techniques displayed in Figure 4.

The refined model value of 4.5195 was also tested for lower ambient pressure conditions, namely  $P = 0.5$  bar. It was found that this did not lead to initial droplet diameters that matched the conclusions of Price *et al.* (2015). Hence the nucleation model had to be refined in terms of sensitivity to ambient pressure and finally an exponent value of 4.658 was chosen for  $P = 0.5$  bar, reducing the droplets to  $D_d = 19.8$   $\mu\text{m}$  at  $T_f = 363$  K,  $P = 0.5$  bar. This condition related to a superheat of 77 K, slightly smaller than that of  $T_f = 393$  K and  $P = 1.0$  bar of 84.9 K, hence the model predicted a slightly larger droplet diameter irrespective of ambient pressure. The predicted spray formation of *n*-pentane after refinement, at three flash-boiling conditions namely,  $T_f = 363$  K and  $P = 0.5$  bar,  $T_f = 393$  K and  $P = 1.0$  bar and  $T_f = 393$  K and  $P = 0.5$  bar is displayed in Figure 14. The conditions were chosen to represent three collapsing spray conditions at increasing superheat degrees taken

from the experimental database of van Romunde *et al.* (2007) and Aleiferis and van Romunde (2013). The focus was aimed at *n*-pentane due to its high volatility and flashing at the experimental conditions investigated. It is also reiterated that gasoline sprays have shown the same type of generic spray collapse mechanism to *n*-pentane as this mechanism is driven by the presence of even low volume fractions of pentanes in gasoline.

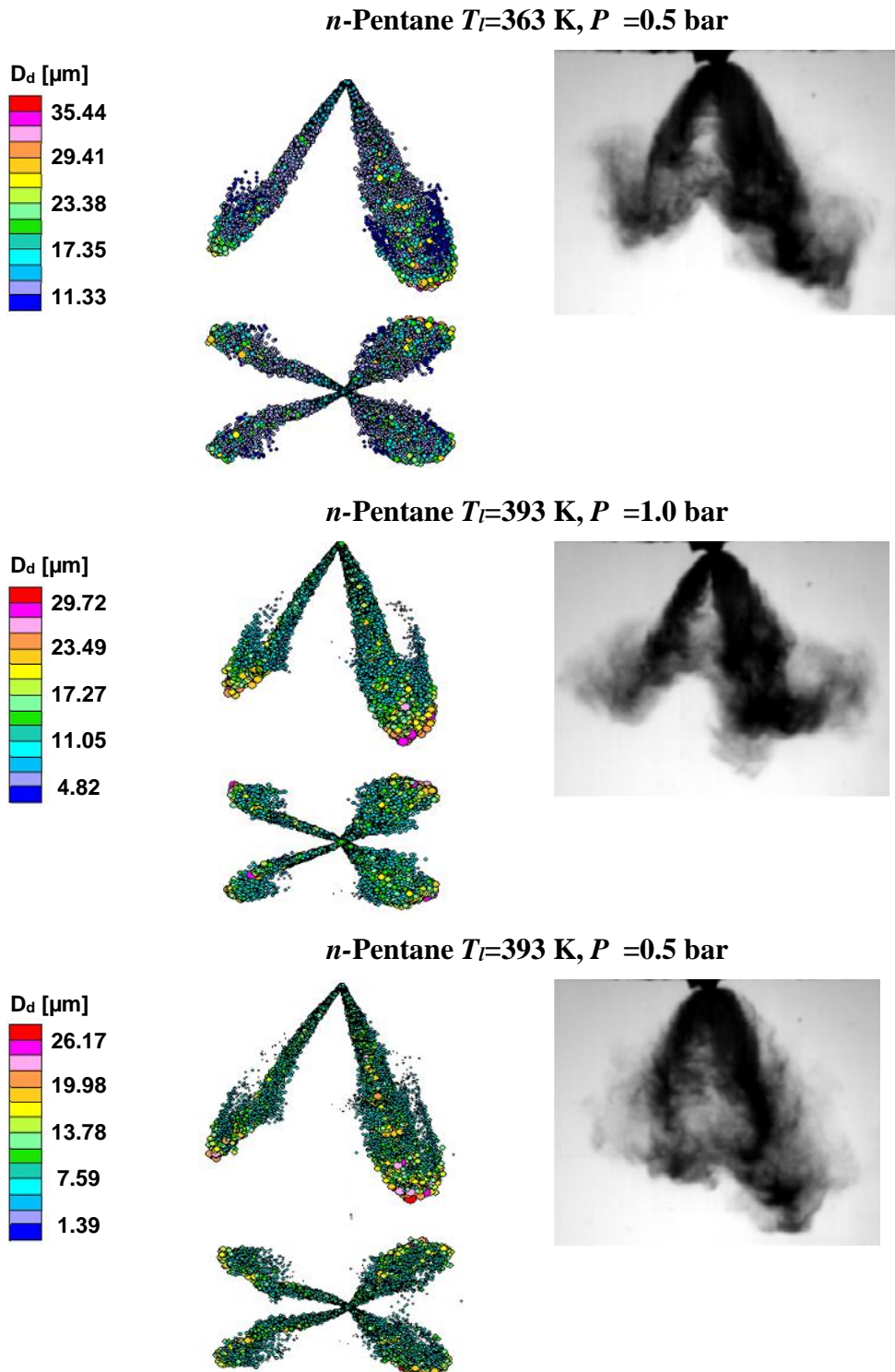


**Figure 14:** Spray formation of flash-boiling *n*-pentane at the following conditions:  $T_l=363$  K and  $P =0.5$  bar,  $T_l=393$  K and  $P =1.0$  bar and  $T_l=393$  K and  $P =0.5$  bar.

As displayed in Figure 14, the flash-boiling atomization model predicts smaller droplets for an increase in superheat regardless of ambient pressure ( $\Delta T=77$  K,  $\Delta T=84.9$  K and  $\Delta T=104$  K

respectively), specifically diameters of  $D_d=19.8 \mu\text{m}$ ,  $D_d=19.1 \mu\text{m}$  and  $D_d=14.0 \mu\text{m}$ , respectively. Even the case of highest superheat with  $D_d=14 \mu\text{m}$  still produced a highly collapsing spray that represented reasonably the experimental observations. It is noted here that in order for the primary atomization model to be able to work within the range of fuel volatilities examined in this paper, at superheats that exceed the order of 100 K, a lower droplet diameter limit is advisable as a boundary condition due to the high sensitivity of the model at very high temperatures. This limit can be set when the initial droplet diameter goes less than about  $14 \mu\text{m}$ ; reducing the initial droplet size to levels even smaller than this led to a rapid change in the general spray characteristics. Therefore, at extreme superheats the effect of superheat itself becomes independent to initial droplet diameter and the spray behaviour is primarily dominated by rapid droplet evaporation. This is an area where further work is needed.

Qualitatively, the spray formation predicted also matches reasonably the behaviour in the experimental shadowgraph images capturing important characteristics. The lack of droplets residing in the central area of the spray is one area that is addressed in a later section, however it has been seen that fuel vapour is drawn into the centre for a collapsing computational spray (Price *et al.*, 2015) as found in experimental studies (Adachi *et al.*, 1996). This can be visualised in Figure 15, whereby the velocity flow field of the continuous phase is plotted on the central plane of symmetry of the injector.

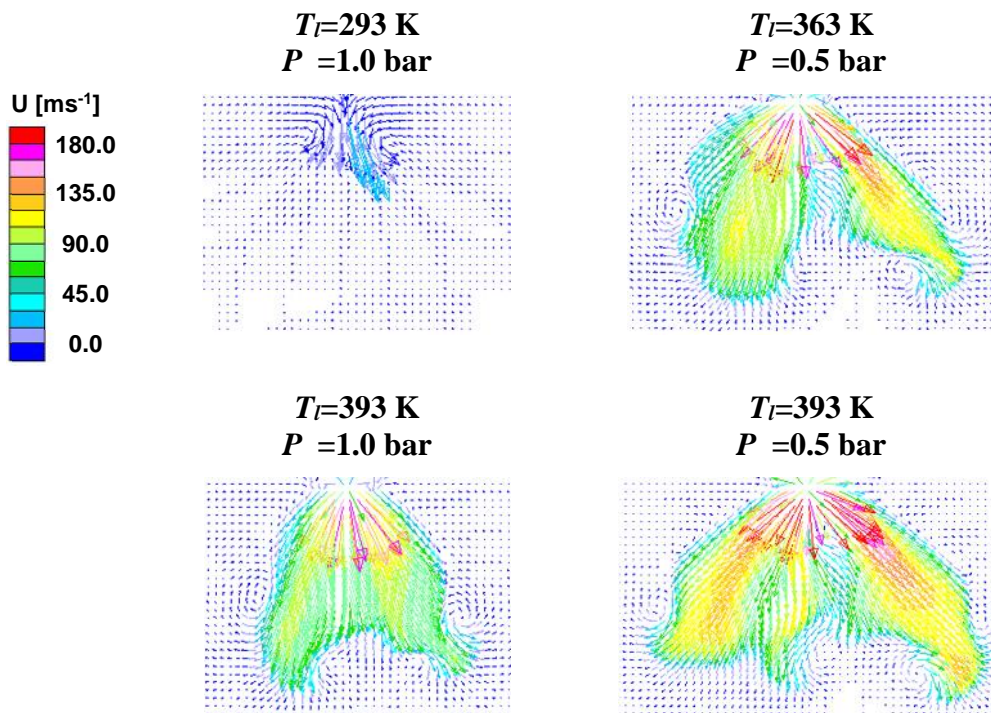


**Figure 15:** Gas velocity on the central plane of the injector for *n*-pentane at  $T_l=293 \text{ K}$  and  $P = 1.0$  bar,  $T_l=293 \text{ K}$  and  $P = 0.5$  bar,  $T_l=393 \text{ K}$  and  $P = 1.0$  bar and  $T_l=393 \text{ K}$  and  $P = 0.5$  bar.

Here a comparison is made to the subcooled, non-flashing spray of *n*-pentane at  $T_l=293 \text{ K}$  and  $P = 1.0$  bar. A significantly larger area is influenced by the spray in terms of velocity at superheated conditions, a result of the collapsing mechanism found as well as an increased injection velocity which produces strong jet tip vortices. These jet tip vortices are clearly displayed in all flash-boiling spray cases. It is interesting to note that the area influenced by the spray is less in the case of  $P = 1.0$  bar. Here a strong vortex is produced on both sides of the spray which is caused by the increased momentum exchange between droplets and surrounding gases, a result of increased gas density and larger drag effects. At superheated conditions, the near nozzle region is typically saturated with

vapour as the evaporation rate at superheat degrees is substantial. This rapid evaporation close to the nozzle exit may also be a cause of the larger influence on gas velocity at superheated conditions.

To understand the code's ability to predict flash-boiling sprays of various fuels after model refinement, *iso*-octane at  $T_l=453$  K  $P =0.3$  bar was investigated using the exponent of 4.5195. The resultant spray is displayed in Figure 16 and compared to the experiment. The code's ability to react to changes in fuel properties is apparent, whereby the most dominant parameter is superheat degree. It can be seen that a strong collapsing mechanism is present, which can be seen by several relatively strong vortices present within close proximity to the plumes. The numerical framework was able to capture severe individual plume collapse, producing two relatively narrow plumes penetrating with large vertical momentum. The degree of droplet shedding from the bulk plumes is somewhat under-predicted, which is likely a result of the fixed plume cone angle and secondary droplet sub-models. This limitation in the near-nozzle spray cone expansion is studied in detail in a subsequent section.

In an attempt to generalise the model over a range of ambient pressures, a pressure dependent relationship for  $y$  is derived through interpolation of the refined exponents at  $P =1.0$  and  $P =0.5$ :

$$y = -3.0 \times 10^{-6}(P_{\infty}) + 4.7965 \quad (30)$$

This relationship allows the model to predict appropriate initial droplet diameters for superheats in the range of  $\Delta T=0-110$  K for *n*-pentane fuel.

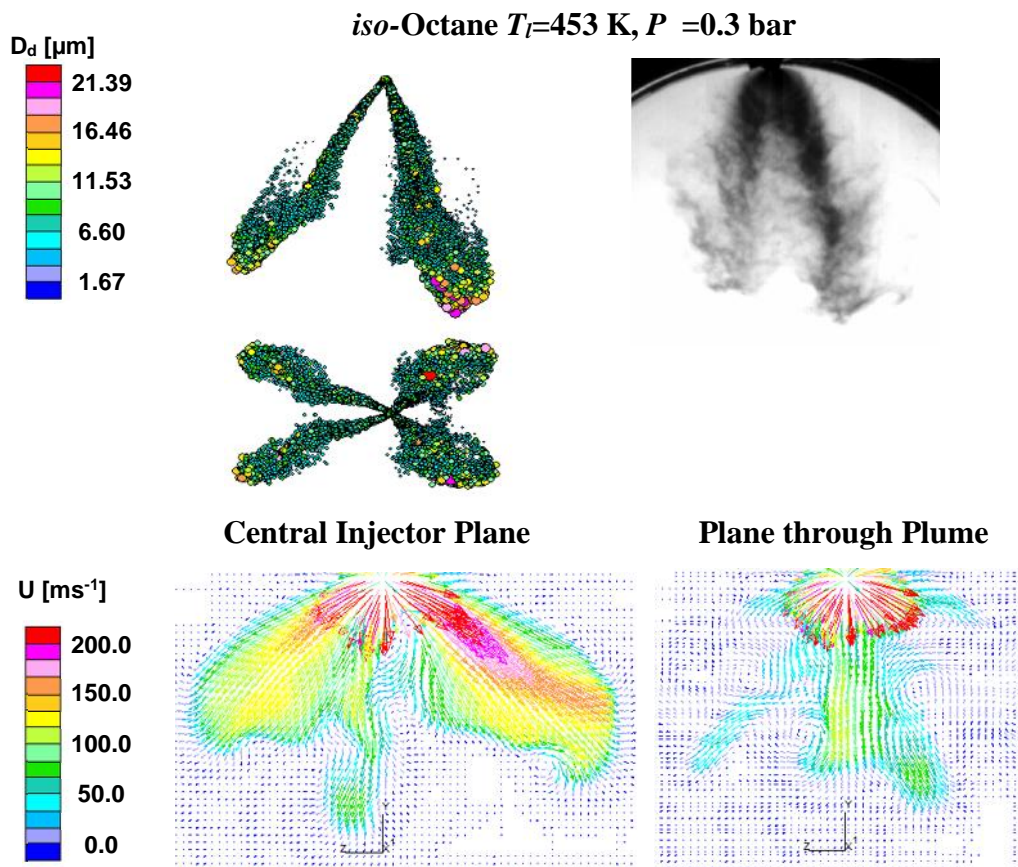


**Figure 16:** Spray formation of *iso*-octane at  $T_l=453$  K  $P =0.3$  bar and gas flow.

To investigate the code's capability to model extremely high superheat conditions, the most extreme case carried out experimentally for *n*-pentane was also simulated here. This condition is  $T_l=453$  K,  $P =0.3$  bar (superheat degree of  $\Delta T=176.1$  K). The resultant spray development is shown in Figure 17 and compared to experiment.

The spray development of the extremely superheated case is somewhat representative of the experimental spray image, whereby two distinct plumes are produced and drawn into the central area. A relatively large spreading of droplets is also captured, however this is under predicted when comparing with the shadowgraph image. Spray formation at both 777  $\mu\text{s}$  and 1177  $\mu\text{s}$  ASOI clearly shows the progression of droplets in the domain, where the plume merging and air entrainment mechanisms produce two relatively even plumes penetrating downwards, as shown in experiment. Several complex vortex structures can be clearly seen in the plane cutting through the plumes, which entrain the small droplets and produce the complex liquid droplet structures predicted. The effect of the added superheat evaporation term is also apparent whereby the majority of droplets were smaller and an increased severity in collapse was predicted as well as high gaseous velocities caused by rapid phase change at the near nozzle region, causing a sudden expansion. It is important to note that a number of droplets are eliminated from the simulation once reaching the codes lower droplet diameter limit. It is clear that such an extreme condition lies at the limits of the current numerical framework. With extremely fast evaporation and saturated cells, a large number of droplets completely evaporate. The physics associated with very high superheat degrees is a novel area, and the current modelling technique may not be a representable approach to such extreme conditions, where the fuel can potentially breach the supercritical limit in the injector body. However, this approach is successful in allowing for a fuel spray to be solved and fuel delivery in the context of engine applications can be achieved.

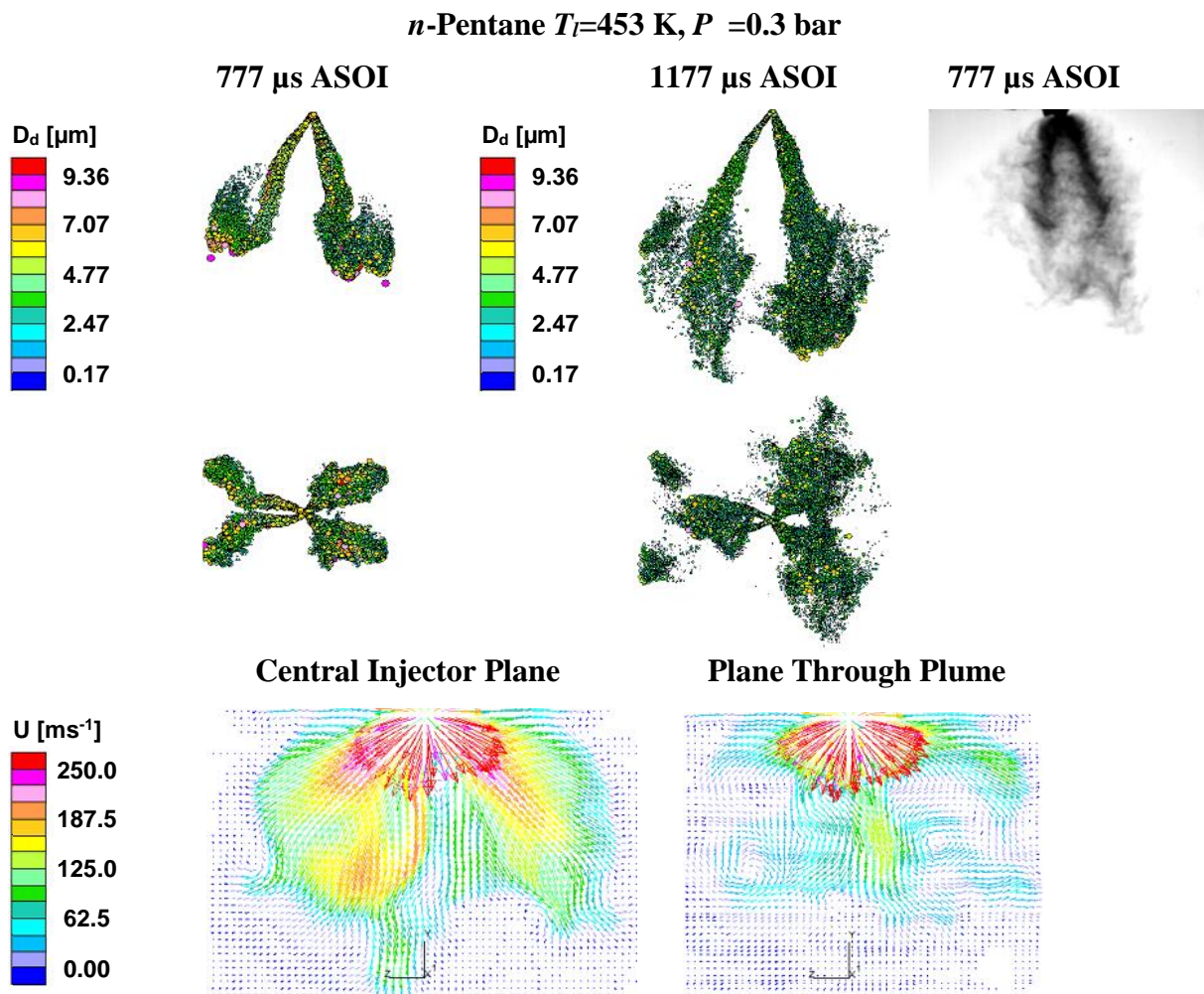


**Figure 17:** Spray formation of *n*-pentane at  $T_I=453$  K,  $P =0.3$  bar. Computational spray at 777  $\mu\text{s}$  and 1177  $\mu\text{s}$  ASOI, experiment at 777  $\mu\text{s}$  ASOI. Gas flow shown at 777  $\mu\text{s}$  ASOI.

## 6. NEAR-NOZZLE PLUME CONE ANGLE

Up until this point the focus has been on the initial droplet diameter, to replicate upstream nucleation and phase-change through the flash-boiling mechanism and the subsequent two-phase flow at the nozzle orifice that would drive spray collapse. A second conclusion from the previous parametric study (Price *et al.*, 2015) states that the individual cone angle is an essential part of replicating all aspects of flash-boiling fuel sprays. Although the general global spray characteristics are captured well using an atomization model in the Lagrangian framework, the near nozzle region is not predicted accurately.

At flash-boiling conditions the individual plume cone angle is significantly increased due to the jet becoming under-expanded causing rapid expansion upon being discharged into the ambient (Oza and Sinnamon, 1983). The cone angle has been found to be highly dependent on superheat degree (Sher and Levi, 2010) due to the nucleation rate being highly dependent on superheat degree. This has also been observed in close up images of the near-nozzle region of the injector under study here (van Romunde *et al.*, 2007; Serras-Pereira *et al.*, 2010; Aleiferis and van Romunde, 2013). The rapid expansion of the vapour phase causes liquid droplets to be entrained radially (Zhifu *et al.*, 2012), increasing the cone angle close to the nozzle exit. A result of this is the distribution of droplets in the spray plume, where larger, heavier droplets remain centrally located due to their larger inertia. Downstream of the nozzle exit, a ‘barrel’ shape is typically found, where droplets follow the surrounding gaseous flow field, being entrained into the central region of the plume and quickly lose radial momentum. The effect of individual plume cone angle on spray characteristics has been previously studied by current authors (Price *et al.*, 2015) whereby an increase in plume cone angle resulted in smaller liquid penetration and a globally smaller SMD. Here a normalised empirical individual cone angle relationship developed by Kamoun *et al.* (2010) is implemented and the resultant spray formation is studied. Firstly, the transition from mechanical to flash-boiling breakup is determined via the critical superheat model of Kitamura *et al.* (1986), whereby dimensionless numbers are used to document the predicted regime, namely a modified Jakob and Weber number. Displayed in Figure 18 are the breakup regimes for both *n*-pentane and *iso*-octane at varying injection temperatures at an injection pressure of  $P_i=150$  bar.

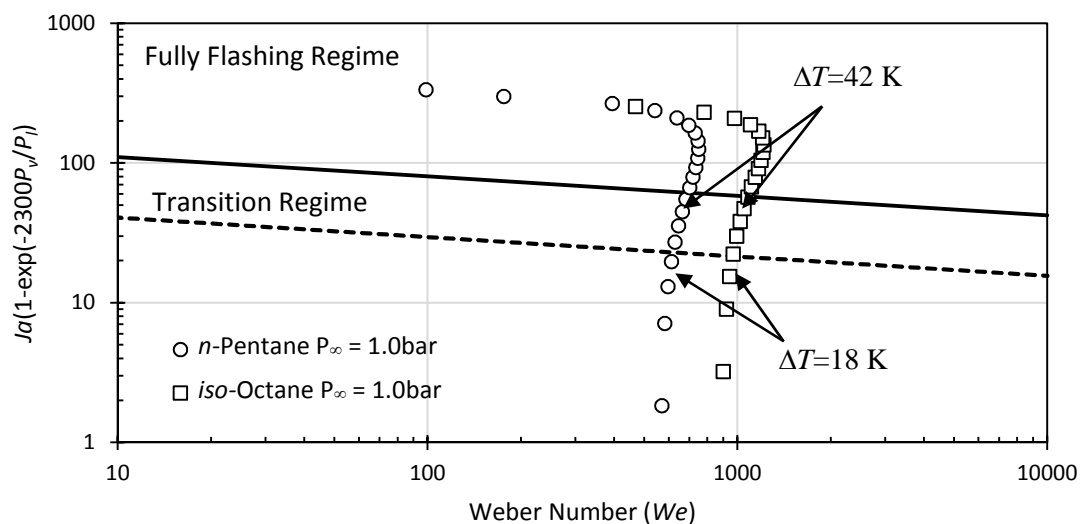


**Figure 18:** Breakup regime transition of *n*-pentane and *iso*-octane fuel sprays with  $P = 1$  bar and  $P_i=150$  bar using the critical superheat model developed by (Kitamura *et al.* 1986).

It is clear that both fuels transition from mechanical to flash-boiling breakup with increasing fuel temperature. As the specific superheat for *n*-pentane and *iso*-octane reaches 42 K, both fuels breach

the fully flashing regime which suggests any condition with a superheat of  $\Delta T > 42$  K is fully flashing. The reader should be aware that the above documented droplet diameter relationship is applied in the Weber number calculation adopted here, hence the reduction in Weber number at high superheat degrees is a result of reducing droplet size. A cone angle relationship derived by Kamoun *et al.* (2010) for fully-flashing sprays is chosen because of the promising normalisation through dimensionless numbers which removes dependency on fuel properties. Adopting the dimensionless term of  $lu$  ( $\frac{R_p^2 \theta^3}{m^2}$ ) where  $R_p$  is the ratio between  $P_s$  and  $P$ , and the dimensionless surface tension originally documented by Girshick and Chiu (1990) and defined as  $\theta = \frac{a_o \sigma}{k_b T_i}$  where  $a_o$  is the molecular surface area and  $k_b$  the Boltzmann constant, a cone angle can be predicted for a range of fuels and operating conditions. The resultant cone angle is plotted against the dimensionless term and displayed in Figure 19.

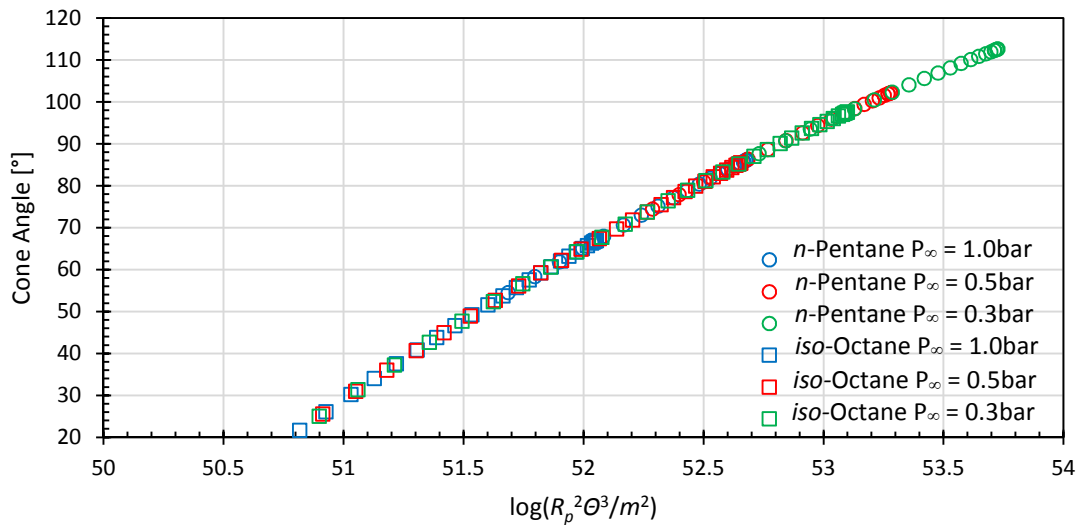


**Figure 19:** Predicted cone angle at varying fuel temperatures and ambient pressures displayed via the dimensionless term of Kamoun *et al.* (2010).

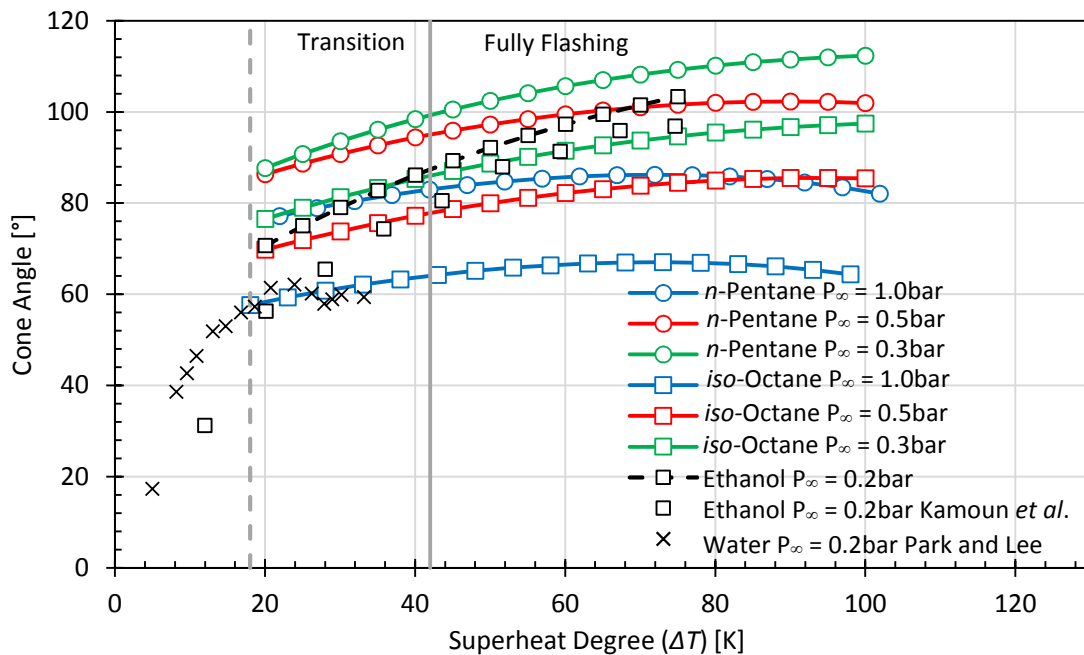


**Figure 20:** Individual plume cone angle of *n*-pentane and *iso*-octane at varying superheat degree and ambient pressure.

The dimensionless logarithmic term collapses all cases onto a single curve. The effect of volatility and superheat degree can be seen by *n*-pentane residing at higher cone angles than *iso*-octane, a consequence of higher superheat degrees at a given temperature. To clearly document the effect of superheat degree and ambient pressure, the cone angle is plotted against superheat degree in Figure 20 and the break-up regimes previously established are documented.

To compare to the experimental results of Kamoun *et al.* (2010) the cone angle relationship was calculated for ethanol fuel at  $P = 0.2$  bar at a distance downstream of the nozzle exit of 20 mm to directly compare. The trend displayed is comparable to the experimental data within 20% at  $\Delta T = 20$  K and 4% at  $\Delta T = 68$  K. A comparison is also made to the experimental work of Park and Lee (1994) where flash-boiling water injected into atmospheric pressure was measured. Here the transition from mechanical break-up to a fully flashing spray can be seen by the steep gradient in cone angle with increasing superheat which plateaus at a superheat of  $\sim 20$  K. It should be noted that the fully flashing regime boundary displayed corresponds to the injection system of the current study and cannot be used for the work of Park and Lee (1994). The fully flashing sprays of Park and Lee (1994) above  $\Delta T > 20$  K produce a cone angle comparable to that calculated for flash-boiling *iso*-octane injected into  $P = 1$  bar of approximately  $60^\circ$  up to the maximum superheat degree studied of 35 K. The reduction in cone angle at high superheat degrees in some cases is a consequence of air entrainment (Kamoun *et al.*, 2010). As superheat increases and droplet diameters subsequently reduce both at the nozzle exit and further downstream, the effect of entrainment becomes more prominent and smaller droplets are drawn further into the central region of the plume resulting in a smaller cone angle at high superheat degrees.

An attempt is made here at studying the code's ability to capture near nozzle phenomena documented in flashing sprays, focusing on the rapid expansion at the nozzle orifice. Firstly, a relatively high superheat degree case is modelled, specifically *n*-pentane at  $T_l = 393$  K  $P = 0.5$  bar ( $\Delta T = 104$  K). The resultant spray formation is displayed in Figure 21. This figure shows that as the jet tip vortices gain strength, the wide initial cone angle quickly reduces due to droplet entrainment in the recirculating gaseous phase. Here four distinct plumes are formed (two plumes are visible from the side view) which occupy a wide area, which is a characteristic seen in the experimental image as well. It has also been seen that plume tips begin to recirculate into the central region at later time-steps, where a distinct curvature of the plume is captured.

All the previous effects of ambient pressure, increased drag forces and spray collapse can be quantified via plotting the liquid penetration. This is displayed in Figure 22. It can be seen that the penetration of the spray set-up with the nominal plume angle of  $15^\circ$  (solid lines) produces penetrations above those of the experimental data, coinciding with the previous sensitivity study of Price *et al.* (2015). The reduced initial droplet diameter predicted via the atomization model reduces the penetration closer to experimental data, a result of increased evaporation, greater deceleration and recirculation at the spray tip. It should also be brought to the reader's attention that an increased injection velocity is used for 393 K as opposed to 363 K ( $125$  and  $115$   $\text{m}\cdot\text{s}^{-1}$ , respectively) due to the reduction in liquid density. Although the injection velocity is larger for the  $T_l = 393$  K cases, the penetration for both  $P = 0.5$  bar is similar, due to higher evaporation rates and smaller predicted droplets for  $T_l = 393$  K. It is also clear that an increase in ambient pressure from  $P = 0.5$  bar to  $P = 1.0$  bar significantly reduces penetration, as expected from larger aerodynamic drag forces acting on the droplets. What is more interesting though, is that with the sub-modelled initial spray cone angle increasing with increased superheat, the predicted penetration curves do match the experimental data to tolerances of the order 5%. This highlights the effect of the near-nozzle axial vs. radial momentum exchange as the superheat is increased and how important it is to include this

effect in the modelling of flashing sprays. As a number of simplifications are still used here, if one applies more accurate boundary conditions in the form of injection rate shaping and droplet size distribution, the numerical results will represent the experimental data even better.

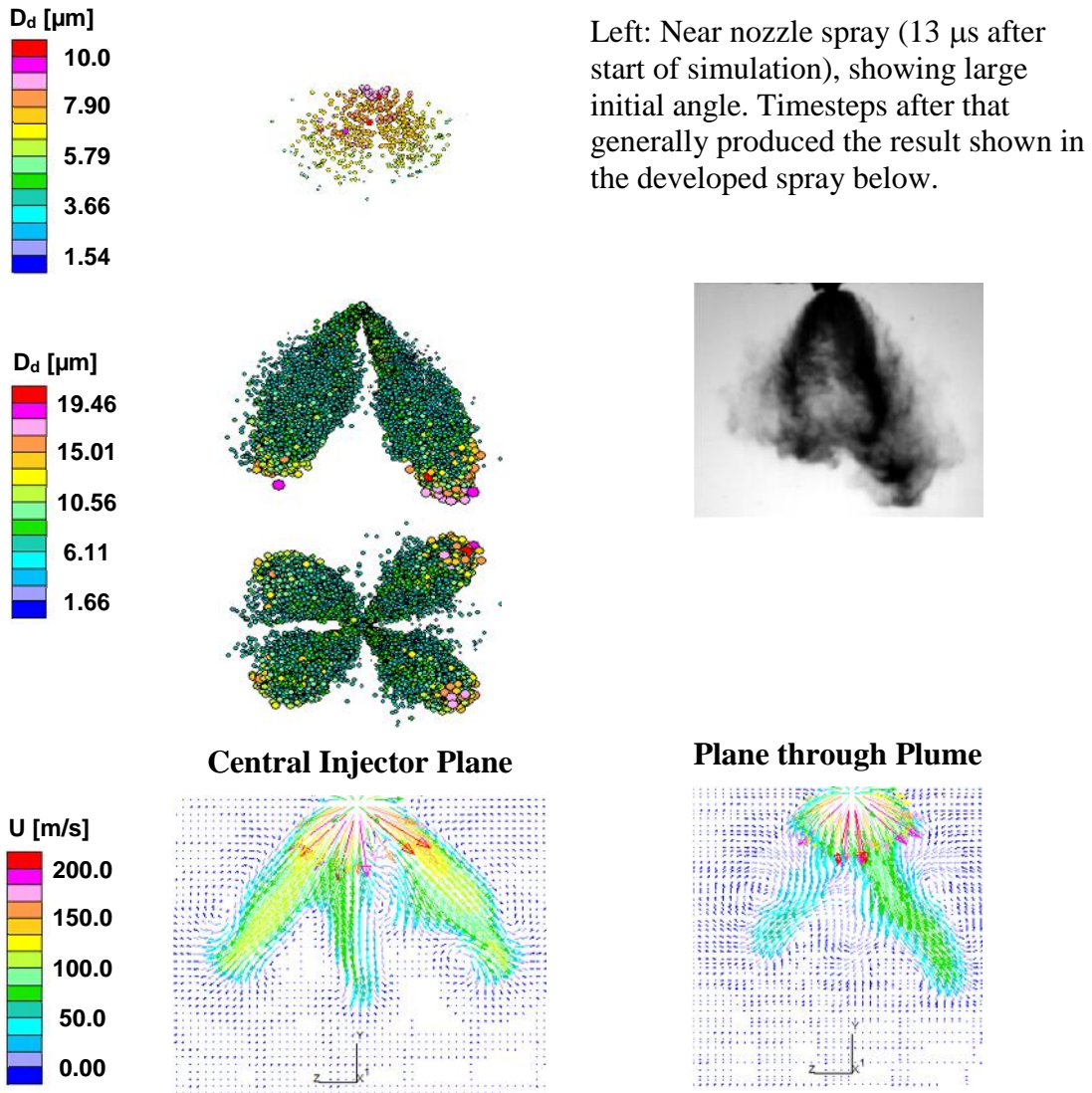


**Figure 21:** Spray of *n*-pentane at  $T_l=393$  K,  $P =0.5$  bar with implemented cone angle.

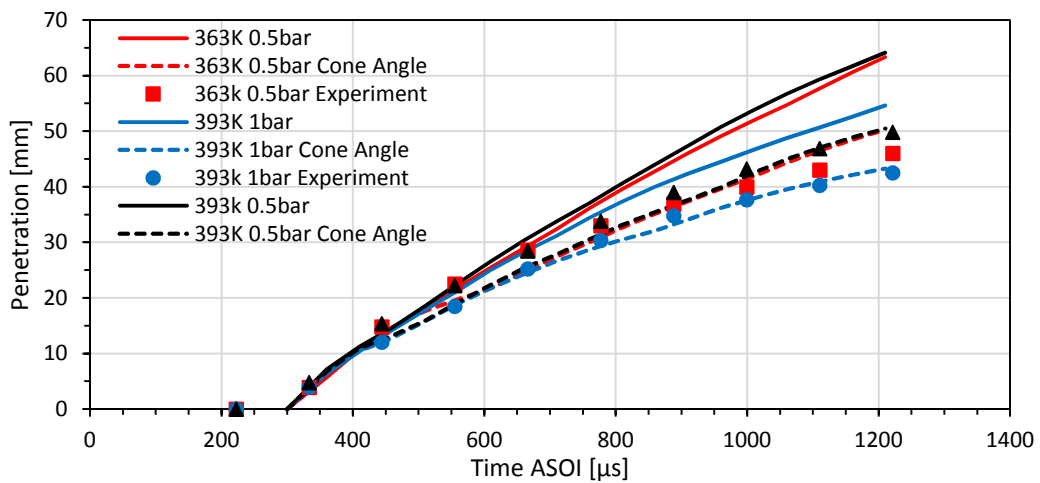


**Figure 22:** Liquid plume penetration of *n*-pentane at  $T_l=363$  K and  $P =0.5$  bar,  $T_l=393$  K and  $P =1.0$  bar and  $T_l=393$  K and  $P =0.5$  bar without and with adjusted cone angle.

The authors also tested the suitability of the current model in another multi-hole injector geometry previously adopted for experimental studies by current authors (see Aleiferis *et al.*, 2009 and 2010b). Results are not displayed here for brevity but the simulations showed agreement over a range of injection temperatures and ambient pressures with the experimental spray collapse pattern of that injector too. Validation against further injector geometries is currently under study and it is believed that the model offers a flexible approach to low-cost simulations of flashing fuel sprays from multi-hole injectors in general.

## 7. CONCLUSIONS

The current work was carried out using an Eulerian/Lagrangian two-phase flow methodology, whereby a zero-dimensional atomization model was implemented to model in-nozzle phase change phenomena from high superheat and applied as a boundary condition at the nozzle exit. Numerically modelled flash-boiling sprays were validated qualitatively and quantitatively against experimental data at a range of superheat degrees of  $\Delta T=77$  K,  $\Delta T=84.9$  K and  $\Delta T=104$  K for flashing *n*-pentane fuel as well as *iso*-octane fuel at a low-pressure high-temperature condition of  $T_l=453$  K and  $P=0.3$  bar. A high superheat condition of *n*-pentane, specifically 176.1 K, was also investigated to study the codes capability at extreme conditions. An empirical cone angle relationship was also investigated. The main conclusions of the current work are as follows:

- A simple nozzle cavitation model cannot really assist on its own the prediction of spray collapse behaviour by simply increasing the superheat and associated vapour pressure.
- An atomization model based on superheated nucleation physics showed capability of predicting a highly reduced initial droplet diameter. Typically, at  $T_l=393$  K  $P=1.0$  bar droplets were reduced to  $\sim 20$   $\mu\text{m}$  from 200  $\mu\text{m}$ .
- Important flash-boiling spray characteristics were captured at a number of flash-boiling conditions. These included plume merging and collapse, and droplet recirculation caused by air entrainment in jet tip vortices.
- A limited approach to modelling extreme flash-boiling cases was also investigated. This was carried out by applying a lower initial droplet diameter limit. In this case (which resides at the limits of the current numerical modelling framework), the dependency on droplet diameter shifts towards a dependency of droplet evaporation which becomes very high at temperatures close to the critical temperature of the fuel.
- The spray shape and liquid penetration were both predicted well at subcooled conditions of  $T_l=293$  K,  $P=1$  bar. However, despite the generally representative overall shape of the spray in terms of collapsing behaviour at increased superheat, the liquid plume penetration was over-predicted by as much as 20–30% at 1 ms ASOI when the initial spray plume cone angle was kept fixed at  $15^\circ$ .
- A sub-model was also implemented for automated nozzle-exit spray cone angle, which increase to typical levels of  $60^\circ$ – $100^\circ$  at increased superheats. With that model included, the liquid penetration eventually matched the experimental data to tolerances of the order 5%. This highlighted the effect of the near-nozzle axial vs. radial momentum balance as the superheat is increased and how important it is to include this effect in the modelling of flashing sprays.

The rapid expansion of vapour upon leaving the nozzle exit is an influential factor in increasing the cone angle. In order to enhance the current simulation capability, this vapour phase behaviour needs to be incorporated into the computational framework. In this context, a change in the radial momentum of child droplets ejected from parent droplets, an effect of rapid bubble growth caused by the sudden depressurisation of the parent droplets, requires specific attention. Current work is

being done to improve the authors' understanding of the near-nozzle flow properties using high-fidelity large-eddy simulation (LES) originating inside the nozzle. For practical implementation at more reasonable computational cost, a coupled in-nozzle LES/Lagrangian approach is also being investigated.

## ACKNOWLEDGEMENTS

Jaguar Land Rover are gratefully acknowledged for the financial and technical support of Christopher James Price via an EPSRC CASE award. EPSRC are also acknowledged for their financial support of Dr. Arash Hamzehloo on research grant number EP/M009424/1. The authors also acknowledge the use of the UCL Legion High Performance Computing Facility (Legion@UCL), and associated support services, in the completion of this work. The authors would also like to thank all members of the UCL Internal Combustion Engines Group for their assistance and many valuable discussions.

## REFERENCES

- Adachi, M., Tanaka, D., Hojyo, Y., Al-Roub, M., Senda., and Fujimoto, H. Measurement of fuel vapor concentration in flash boiling spray by infrared extinction/scattering technique. *JSAE Review*, Vol. 17, pp. 231–237, 1996.
- Adachi, M., McDonell, V., and Tanaka, D. Characterization of fuel vapor concentration inside a flash boiling spray. *SAE Paper 970871*, 1997.
- Aleiferis, P. G., Serras-Pereira, J., van Romunde, Z., and Caine, J. Spray development in E85 and gasoline in a quiescent chamber and in direct-injection spark-ignition engine. *Proceedings of the Fourth International Conference on Thermal Engineering: Theory and Applications*, Abu Dhabi, UAE, 2009.
- Aleiferis, P. G., Serras-Pereira, J., Augoye, A., Davies, T. J., Cracknell, R. F., and Richardson, D. Effect of Fuel Temperature on In-Nozzle Cavitation and Spray Formation of Liquid Hydrocarbons and Alcohols from a Real-Size Optical Injector for Direct-Injection Spark-Ignition Engines. *International Journal of Heat and Mass Transfer*, Vol. 53, pp. 4588–4606, 2010.
- Aleiferis, P. G., Serras-Pereira, J., van Romunde, Z., Caine, J., and Wirth, M. Mechanisms of spray formation and combustion from a multi-hole injector with E85 and gasoline. *Combustion and Flame*, Vol. 157, pp. 735–756, 2010b.
- Aleiferis, P. G. and van Romunde, Z. R. An Analysis of Spray Development with *iso*-Octane, *n*-Pentane, Gasoline, Ethanol and *n*-Butanol from a Multi-Hole Injector under Hot Fuel Conditions. *Fuel*, Vol. 105, pp. 143–168, 2013.
- Ashgriz, N. *Handbook of atomization and sprays theory and applications*. London: Springer, 2011.
- Behringer, M. K., Aleiferis, P. G., OudeNijeweme, D., and Freeland, P. Spray Formation from Spark-Eroded and Laser-Drilled Injectors for DISI Engines with Gasoline and Alcohol Fuels. *SAE International Journal of Fuels and Lubricants*, Vol. 7, pp. 803–822, *SAE Paper 2014-01-2745*, 2014.
- Behringer, M. K., Aleiferis, P. G., OudeNijeweme, D. and Freeland, P., Spray Imaging and Droplet Sizing of Spark-Eroded and Laser-Drilled Injectors with Gasoline-Butanol and Gasoline-Ethanol Blends, *International Conference on Fuel Systems for IC Engines*, IMechE, London, pp. 179–198, 2015.
- Bird, R., Stewart, W., and Lightfoot, E. *Transport phenomena*. John Wiley and sons, 1966.

- Blander, M., and Katz, J. Bubble nucleation in liquids. *AIChE Journal*, Vol. 10, pp. 1–32, 1979.
- Blinkov, V.N., Jones, O.C. and Nigmatulin, B.I., 1993. Nucleation and flashing in nozzles – 2. Comparison with experiments using a five-equation model for vapor void development. *International Journal of Multiphase Flow*, Vol. 19, pp. 965–986.
- Brennen, C. E. *Cavitation and Bubble Dynamics*. Oxford University Press, New York, 1995.
- Brown, R. L. and Stein, S.E. Boiling Point Data in NIST Chemistry WebBook, NIST Standard Reference Database Number 69, Eds. P.J. Linstrom and W.G. Mallard. National Institute of Standards and Technology, Gaithersburg MD, 20899, <http://webbook.nist.gov>
- Butcher, A. J., Aleiferis, P.G., and Richardson, D. Development of a real-size optical injector nozzle for studies of cavitation, spray formation and flash-boiling at conditions relevant to direct-injection spark-ignition engines. *International Journal of Engine Research*, Vol. 14, pp. 557–577, 2013.
- Butcher, A.J., Aleiferis, P.G., and Richardson, D. Characterisation of Spray Development from Spark-Eroded and Laser-Drilled Multi-hole Injectors in an Optical DISI Engine and in a Quiescent Injection Chamber. SAE Paper 2015-01-1903, 2015.
- Cole, R. Bubble frequencies and departure volumes at subatmospheric pressures. *AIChE Journal*, Vol. 13, pp. 779–783, 1967.
- Delale, C.F., Schnerr, G.H. and Sauer, J. Quasi-one-dimensional steady-state cavitating nozzle flows. *Journal of Fluid Mechanics*, Vol. 427, pp. 167–204, 2001.
- Girshick, S.L., and Chiu, C.P. Kinetic nucleation theory: A new expression for the rate of homogeneous nucleation from an ideal supersaturated vapor. *The Journal of Chemical Physics*, Vol. 93, pp. 1273–1277, 1990.
- Issa R. I. Solution of the implicitly discretised fluid flow equations by operator-splitting. *J. Computational physics*. Vol. 62, pp. 40-65, 1986.
- Janet, J.P., Liao, Y. and Lucas, D. Heterogeneous Nucleation in CFD Simulation of Flashing Flows in Converging-Diverging Nozzles. *International Journal of Multiphase Flow*. Vol. 74, pp. 106–117, 2015.
- Kamoun, H. Lamanna, G., Weigand, B. High-speed shadowgraphy investigations of superheated liquid jet atomisation. ILASS-Americas 22<sup>nd</sup> Annual Conference on Liquid Atomization and Spray Systems, Cincinnati, USA, 2010.
- Kitamura, Y., Morimitsu, H., and Takahashi, T. Critical superheat for flashing of superheated liquid jets. *Industrial and Engineering Chemistry Fundamentals*, Vol. 25, pp. 206–211, 1986.
- Kocamustafaogullari, G., and Ishii, M. Interfacial area and nucleation site density in boiling systems. *International Journal of Heat and Mass Transfer*, Vol. 26, pp. 1377-1387, 1983.
- Kurul, N., and Podowski, M. On the modelling of multidimensional effects in boiling channels. In *ANS Proc. 27<sup>th</sup> National Heat Transfer Conference*, Minneapolis, USA, MN, Springer-Verlag. pp. 28–31, 1991.
- Lemmert, M., and Chawla, J. Influence of flow velocity on surface boiling heat transfer coefficient. In: Hahne, E., Grigull, U. (Eds.), *Heat Transfer in Boiling*, pp. 237–247, Hemisphere, 1977.
- Li, S., Zhang, Y. and Xu, B. Correlation analysis of superheated liquid jet breakup to bubble formation in a transparent slit nozzle. *Experimental Thermal and Fluid Science*, Vol. 68, pp. 452–458, 2015.

- Lichtarowicz, A., Duggins, R.K., and Markland, E. Discharge Coefficients for Incompressible Non-Cavitating Flow through Long Orifices. *Journal of Mechanical Engineering Science*, Vol. 7, pp. 210–219, 1965.
- Neroorkar, K., Gopalakrishnan, S., Grover, R.O., Schmidt, D.P. Simulation of Flash Boiling in Pressure Swirl Injectors. *Atomization and Sprays*, Vol. 21, pp. 179–188, 2011.
- Neroorkar, K., and Schmidt, D. Modelling of vapor-liquid equilibrium of gasoline-ethanol blended fuels for flash boiling simulations. *Fuel*, Vol. 90, pp. 665–673, 2011.
- Nurick, W.H. Orifice Cavitation and Its Effect on Spray Mixing. *Journal of Fluids Engineering*, Vol. 98, pp. 681–687, 1976.
- Oza, R. and Sinnamon, J., 1983. An experimental and analytical study of flash-boiling fuel injection. SAE Paper 830590, 1983.
- Park, B., and Lee, S. An experimental investigation of the flash atomization mechanism. *Atomization and Sprays*, Vol. 4, pp. 159–179, 1994.
- Payri, R., Guardiola, C., Salvador, F.J., Gimeno., J. Critical cavitation number determination in diesel injection nozzles. *Experimental Techniques*, Vol. 28, pp. 49–52, 2004.
- Payri, R., Guardiola, C., Salvador, F.J., Gimeno., J. Using spray momentum flux measurements to understand the influence of diesel nozzle geometry on spray characteristics. *Fuel*, Vol. 84, pp. 551–561, 2005.
- Price, C., Hamzehloo, A., Aleiferis, P.G., and Richardson, D. Aspects of Numerical Modelling of Flash-Boiling Fuel Sprays. SAE Paper 2015-24-2463, 2015.
- Riznic, J., and Ishii, M. Bubble number density and vapor generation in flashing flow. *International Journal of Heat and Mass Transfer*, Vol. 32, 10, pp. 1821–1833, 1989.
- Sarre, C.V.K., Kong, S., and Reitz, R.D. Modeling the Effects of Injector Nozzle Geometry on Diesel Sprays. SAE Paper 1999-01-0912, 1999.
- Schmidt, D.P., and Corradini, M.L. The internal flow of diesel fuel injector nozzles: a review. *International Journal of Engine Research*, Vol. 2, pp. 1–22, 2001.
- Schmidt, D.P., and Rutland, C. A new droplet collision algorithm. *Journal of Computational Physics*, Vol. 164, pp. 62–80, 2000.
- Serras-Pereira, J., Aleiferis, P. G., Richardson, D., and Wallace, S. (2007). Mixture Formation and Combustion Variability in a Spray-Guided DISI Engine. SAE Transactions, *Journal of Engines*, Vol. 116, pp. 1332–1356, SAE Paper 2007-01-4033, 2007.
- Serras-Pereira, J., Aleiferis, P. G., Richardson, D., and Wallace, S. Characteristics of Ethanol, Butanol, *iso*-Octane and Gasoline Sprays and Combustion from a Multi-Hole Injector in a DISI Engine. SAE International *Journal of Fuels and Lubricants*, Vol. 1, pp. 893–909, SAE Paper 2008-01-1591, 2008.
- Serras-Pereira, J., van Romunde, Z., Aleiferis, P.G., Richardson, D., Wallace, S., and Cracknell, R.F. Cavitation, primary break-up and flash boiling of gasoline, *iso*-octane and *n*-pentane with a real-size optical direct-injection nozzle. *Fuel*, Vol. 89, pp. 2592–2607, 2010.
- Serras-Pereira, J., Aleiferis, P.G., and Richardson, D. Imaging and Heat Flux Measurements of Wall Impinging Sprays of Hydrocarbons and Alcohols in a Direct-Injection Spark-Ignition Engine. *Fuel*, Vol. 91, pp. 264–297, 2012.

- Serras-Pereira, J., Aleiferis, P. G., Walmsley, H. L., Davies, T. J., and Cracknell, R. F. Heat Flux Characteristics of Spray Wall Impingement with Ethanol, Butanol, *iso*-Octane, Gasoline and E10 Fuels. *International Journal of Heat and Fluid Flow*, Vol. 44, pp. 662–683, 2013.
- Serras-Pereira, J., Aleiferis, P.G., and Richardson, D. An experimental database on the effects of single- and split injection strategies on spray formation and spark discharge in an optical direct-injection spark-ignition engine fuelled with gasoline, *iso*-octane and alcohols. *International Journal of Engine Research*, Vol. 16, pp. 851–896, 2015.
- Shepherd, J. E., and Sturtevant, B. Rapid evaporation at the superheat limit. *Journal of Fluid Mechanics*, Vol. 121, pp. 379 – 402, 1982.
- Sher, E., Bar-Kohany, T., and Rashkovan, A. Flash-boiling atomization. *Progress in Energy and Combustion Science*, Vol. 34, pp. 417–439, 2008.
- Sher, E., and Elata, C. Spray Formation from Pressure Cans by Flashing. *Industrial and Engineering Chemistry Process Design and Development*, Vol. 16, pp. 237–242, 1977.
- Sher, E. and Levi, M. Spray Formation from Homogeneous Flash-Boiling Liquid Jets. 23<sup>rd</sup> Annual Conference on Liquid Atomization and Spray Systems (ILASS), Brno, Czech Republic, 2010.
- Shiller, L. and Neumann, A., 1933. Über die grundlegenden Berechnungen bei der Schwerkraftaufbereitung. *VDI Zeits*, Vol. 77, pp. 318-320.
- Shin, T.S. and Jones, O.C., 1993. Nucleation and flashing in nozzles – 1. *International Journal of Multiphase Flow*, Vol. 19, pp. 943–964.
- Spalding, D.B. The combustion of liquid fuels. *Symposium (International) on Combustion*. Vol. 4, pp. 847–864, 1953.
- van Romunde, Z., Aleiferis, P.G., Cracknell, R. Effect of fuel properties on spray development from a multi-hole DISI engine injector. *SAE Transactions, Journal of Engines*, Vol. 116, pp. 1313–1331, SAE Paper 2007-01-4032, 2007.
- van Romunde, Z.R. and Aleiferis, P.G. Effect of Operating Conditions and Fuel Volatility on Development and Variability of Sprays from Gasoline Direct-Injection Multi-Hole Injectors. *Atomization and Sprays*. *Atomization and Sprays*, Vol. 19, pp. 207–234, 2009.
- Vieira, M.M. and Simões-Moreira, J.R. Low-pressure flashing mechanisms in *iso*-octane liquid jets. *Journal of Fluid Mechanics*, Vol. 572, pp.121–144, 2007.
- Witlox, H.W.M., and Bowen, P.J. *Flashing Liquid Jets and Two-Phase Dispersion – A Review*. HSE Books, 2002.
- Xu, B.Y., Zhang, X.C., Xu, J., Qi, Y.L., Cai, S.L. Numerical analysis of homogeneous mixture formation for a direct injection liquid LPG engine. *International Journal of Automotive Technology*, Vol. 14, pp. 857–865, 2013.
- Yakhot, V., Orszag, S.A., Thangam, S., Gatski, T.B., Speziale, C.G. Development of turbulence models for shear flows by a double expansion technique. *Physics of Fluids*, Vol. 4, pp. 1510–1520, 1992.
- Yaws, C.L. *Yaws' handbook of thermodynamic and physical properties of chemical compounds: physical, thermodynamic and transport properties for 5,000 organic chemical compounds*. Knovel, 2003.
- Zhang, G., Xu, M., Zhang, Y., Zeng, W. Quantitative Measurements of Liquid and Vapor Distributions in Flash Boiling Fuel Sprays using Planar Laser Induced Exciplex Technique, *SAE Paper* 2011-01-1879, pp. 1728–1735, 2011.

Zhang, M., Xu M., Zhang Y., Zhang G., and Cleary D. J. Flow-Field Investigation of Multihole Superheated Sprays Using High-Speed PIV. Part II. Axial Direction. *Atomization and Sprays*, Vol. 23, pp. 119-140, 2013.

Zhang, Y., Shiyan, L., Zheng, B., Wu, J., Xu, B. Quantitative observation on breakup of superheated liquid jet using transparent slit nozzle. *Experimental Thermal and Fluid Science*, Vol. 63, pp. 84–90, 2015.

Zhifu, Z., Weitao, W., Bin, C., Guoxiang, W., Liejin, G. An experimental study on the spray and thermal characteristics of R134a two-phase flashing spray. *International Journal of Heat and Mass Transfer*, Vol. 55, pp. 4460–4468, 2012.